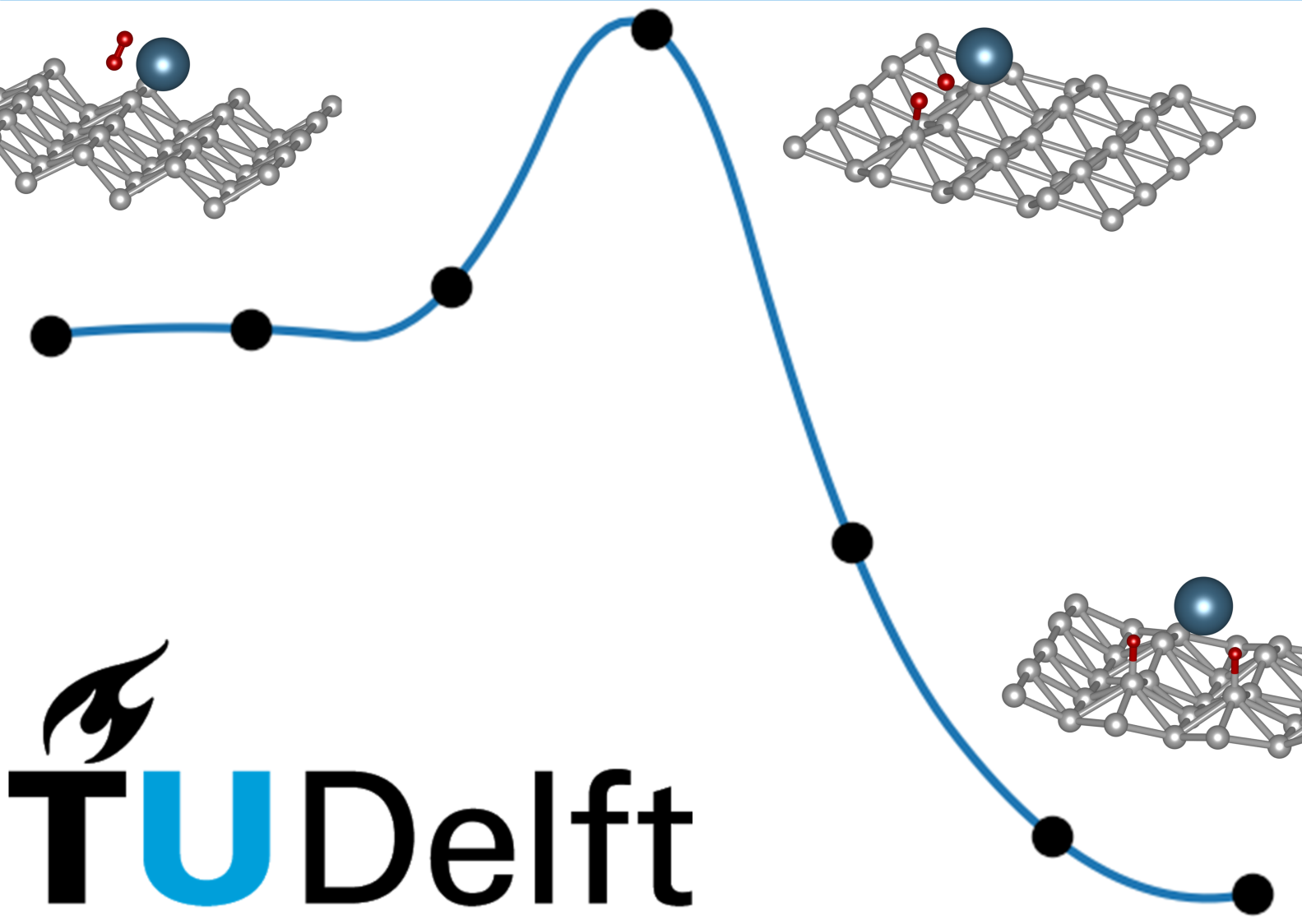


DFT based study of hydrogen adsorption and desorption on borophene structures

Tijin Hanno Geo Saji



DELFT UNIVERSITY OF TECHNOLOGY

DFT based study of hydrogen adsorption and desorption on borophene systems

By:

Tijin Hanno Geo SAJI
(Student number: 5010322)

Daily Supervisor:

Parsa HABIBI, MSE and P&E, TU Delft

Thesis Committee:

Dr. Othon MOULTOS, P&E, TU Delft
Dr. Poulumi DEY, MSE, TU Delft
Dr. Carey WALTERS, M&TT, TU Delft

*A thesis submitted in fulfillment of the requirements
for the degree of Master of Science in Materials Science and
Engineering*

in the

Department of Materials Science and Engineering



Materials Science
and Engineering



“For by You I can run against a troop, By my God I can leap over a wall.”

Psalm 18:29

Abstract

Climate change is one of the top global issues that the United Nations has identified that can adversely impact people all around the globe. Moving towards a hydrogen economy can reduce greenhouse emissions produced from burning fossil fuels which is one of the biggest contributors to global warming and climate change. Hydrogen fuel has a high gravimetric density and being a clean fuel it has the potential to become a sustainable energy source for the growing market. However, its low volumetric density makes it a difficult fuel to store, thus making storage technologies in the hydrogen supply chain an important part.

The current storage technologies, however, are impeded by shortcomings such as low hydrogen densities, extreme pressure and temperature operating conditions and inefficiencies during the storage process. Combining existing hydrogen storage technologies such as compressed hydrogen gas and metal hydrides with 2D materials comes across as an excellent option as they can complement each other in their functioning. In this regard, borophene is considered a viable material for hydrogen storage due to its lightweight, good thermal, mechanical and electrical properties. Most of the studies performed so far on hydrogen storage in borophene were on hydrogen physisorption via weak van der Waals forces. In this thesis work, the chemisorption of hydrogen on borophene via strong covalent bonds is studied. This is because borophene with chemisorbed hydrogen is more energetically stable than with physisorbed hydrogen. Also, chemisorbed hydrogen on borophene performs better than physisorbed hydrogen in terms of safety and long-term storage.

Hydrogen chemisorption on pristine, defective (i.e. with single and double vacancies) and metal decorated borophene are studied in this work, using density functional theory (DFT) and nudged elastic band (NEB) calculations to compute quantities such as enthalpy and activation energy barriers of chemisorption. Using Bader charge analysis and partial density of states analysis, it was observed that the addition of charge on the hydrogen bond weakens the bond, expediting the chemisorption reaction. The charge transfer from borophene to the chemisorbed H atoms was found to stabilize the final chemisorbed state. In the case of metal decorations, there is an additional steric factor that influences the activation barrier height for chemisorption. In general, metal decorations performed better than pristine and defective borophene systems in terms of the desorption barrier height, among which double decorated K atoms on borophene substrate had the best performance, improving the barrier height by 20% compared to the corresponding value for the pristine system.

Acknowledgement

I give all glory and honor to my Almighty God for giving me grace and strength to complete my thesis work. Without His lovingkindness and tender mercies, I could not have come this far.

I would like to thank my supervisors, Dr. Othon Moulton, Dr. Poulumi Dey and Parsa Habibi, for their constant guidance and assistance throughout my master thesis work. A journey I thought would be rough and difficult was made easy and enjoyable by their support. I would like to express my gratitude to Dr. Carey Walters for agreeing to be a part of the thesis committee.

I would like to thank Appa, Amma, Tibin and Tabitha for their constant support throughout. Also special thanks to my best friend Sheryl, who has been with me all through the journey. I can't thank enough my friend Sarika, who has been a constant source of support and has helped me during some real tough times. Special thanks to Narasimhan who shared his experience on his DFT based thesis work. And my friends in Delft, Jonathan, Surya, Anjana, Viswanath, Naveen, Aswathi, Avanika, thank you to you guys as well for those nice get together parties and the food.

I would like to take this time to also thank my prayer group friends, Yonatan, Jonathan, Eldhose and Ammani. Those weekend prayers were a real source of support for me.

I would also like to thank my 'lab partners' in the hpc cluster, whom I know only by their usernames seen on my black PuTTY screen. Thanks to you all as well for allowing me to run my heavy NEB calculations on the shared nodes.

Contents

Abstract	ii
Acknowledgements	iii
1 Introduction	1
1.1 Outline of report	2
2 Scientific background	3
2.1 Existing technologies for hydrogen storage	3
2.2 2D materials	5
2.2.1 Borophene structures	5
2.3 Physisorption on borophene	6
2.4 Simulation studies on chemisorption	6
2.5 Research questions	7
3 Methodology	8
3.1 Density functional theory	8
3.1.1 Overview	8
3.1.2 Kohn-Sham approach	8
Energy Terms	9
Exchange-Correlation functionals	10
Pseudopotential	11
Solving Kohn-Sham equations	11
3.2 Nudged elastic band method	12
3.3 Vienna ab initio simulation package	13
3.3.1 Input files	13
3.4 Input tags	13
3.4.1 KPOINTS	14
3.4.2 ENCUT	14
ISMEAR	15
3.4.3 IVDW	16
3.4.4 System size effects	16
3.4.5 Input parameters	17
3.4.6 Energy profile and associated terms	18
4 Results and Discussion	19
4.1 Pristine	19
4.2 Vacancies	20
4.3 Metal decoration	24
4.4 Double metal decorations	27

4.5	Discussion	29
4.5.1	Range of energies	29
4.5.2	Charge transfer	30
4.5.3	Adsorption energies	31
4.5.4	Distances and bond lengths	31
	D _{H-H} values	31
	D _{B-H} values	32
4.5.5	Density of states	33
4.5.6	ΔH_{ads} , $E_{\text{ads-bar}}$ and $E_{\text{des-bar}}$ values	34
4.5.7	Possible applications	34
5	Conclusion	36
6	Recommendations	38
A	Configurations	40
A.1	Pristine	40
A.2	Single vacancy	40
A.3	Double vacancy	40
B	Bash scripts	46
C	NEB of metal decorations	47
D	Sensitivity analysis	51
E	VASP Primer	52
	Bibliography	57

List of Figures

1.1	Production and storage methods of hydrogen [3].	2
2.1	Available hydrogen storage methods [6].	3
2.2	Joule-Thomson coefficient of H, He and N [9].	4
2.3	Commonly studied borophene structures- (a) β_{12} , (b) χ_3 and (c) 2- <i>Pmmn</i> (striped) borophene [21].	5
3.1	Contributions of the energy terms for an He atom [38].	10
3.2	Flowchart for solving KS equations [38].	12
3.3	Potential energy landscape of the reaction whose initial, intermediary and final states are shown [38].	13
3.4	KPOINTS convergence of a 4×5 pristine borophene supercell with an ENCUT value of 500 eV.	15
3.5	ENCUT convergence of a 4×5 pristine borophene supercell with KPOINTS of $5 \times 5 \times 1$	15
3.6	Energy profile of a chemisorption reaction on a pristine borophene system with the associated terms labeled.	18
4.1	(a) Physisorbed and (b) chemisorbed states of H_2 on pristine borophene. Grey spheres represent B atoms while red spheres represent H atoms.	19
4.2	Minimum energy pathway corresponding to H_2 dissociation on pristine borophene. For the reaction, the ΔH_{ads} and $E_{ads-bar}$ was found to be -1.39 eV and 0.76 eV respectively. The blue dots are the NEB images while the red line connecting the blue dots is a guide to the eye. The NEB images in this report are generated from the scripts provided by the Henkelman group [44].	21
4.3	(a) Physisorbed and (b) chemisorbed states of H_2 on single vacancy borophene.	22
4.4	(a) Physisorbed and (b) chemisorbed states of H_2 on double vacancy borophene.	23
4.5	Minimum energy pathway corresponding to H_2 dissociation on single vacancy borophene. For the reaction, the ΔH_{ads} and $E_{ads-bar}$ was found to be -1.53 eV and 0.69 eV respectively.	23
4.6	Minimum energy pathway corresponding to H_2 dissociation on double vacancy borophene. For the reaction, the ΔH_{ads} and $E_{ads-bar}$ was found to be -1.48 eV and 0.62 eV respectively.	24

4.7	(a) Physisorbed and (b) chemisorbed states of H ₂ on K decorated borophene. Grey spheres represent B atoms, red spheres, H atoms and K atoms are represented by purple spheres. . . .	26
4.8	Minimum energy pathway corresponding to H ₂ dissociation on K decorated borophene. For the reaction, the ΔH_{ads} and $E_{\text{ads-bar}}$ was found to be -1.11 eV and 0.68 eV respectively. . . .	27
4.9	(a) Physisorbed and (b) chemisorbed states of H ₂ on double K decorated borophene.	28
4.10	Minimum energy pathway corresponding to H ₂ dissociation on double K decorated borophene. For the reaction, the ΔH_{ads} and $E_{\text{ads-bar}}$ was found to be -1.00 eV and 0.73 eV respectively. . . .	29
4.11	Product of charge on H atoms for the various systems studied.	30
4.12	Adsorption energies of H ₂ on various systems studied.	31
4.13	Distance between H atoms for the various systems studied.	32
4.14	Distance between borophene and the H atoms for the various systems studied.	32
4.15	PDOS of B(p) and H(s) in H ₂ physisorbed pristine borophene system with the black vertical line being the Fermi level. . . .	33
4.16	PDOS of B(p) and H(s) in H ₂ chemisorbed pristine borophene system with the black vertical line being the Fermi level. . . .	33
4.17	ΔH_{ads} , $E_{\text{ads-bar}}$ and $E_{\text{des-bar}}$ values of the systems studied. . . .	34
A.1	Configurations for pristine physisorption.	40
A.2	Configurations for pristine chemisorption.	41
A.3	Configurations for SV physisorption.	42
A.4	Configurations for SV chemisorption.	43
A.5	Configurations for DV physisorption.	44
A.6	Configurations for DV chemisorption.	45
B.1	Script to obtains energies from folders within.	46
B.2	Script to obtains time taken for calculations from folders within.	46
C.1	Minimum energy pathway corresponding to H ₂ dissociation on Ca decorated borophene.	47
C.2	Minimum energy pathway corresponding to H ₂ dissociation on Li decorated borophene.	48
C.3	Minimum energy pathway corresponding to H ₂ dissociation on Na decorated borophene.	48
C.4	Minimum energy pathway corresponding to H ₂ dissociation on double Ca decorated borophene.	49
C.5	Minimum energy pathway corresponding to H ₂ dissociation on double Li decorated borophene.	49
C.6	Minimum energy pathway corresponding to H ₂ dissociation on double Na decorated borophene.	50
D.1	Time taken for Gaussian, MP-1 and MP-2 smearing for a range of SIGMA values.	51
E.1	Login window	52

E.2	After login window	52
E.3	Making a new directory	53
E.4	Changing directory	53
E.5	Creating files	53
E.6	KPOINTS for pristine borophene	54
E.7	INCAR for pristine borophene	54
E.8	POSCAR for pristine borophene	55
E.9	Submit job script	56
E.10	Submit job script with white background	56

List of Tables

2.1	Density Functional Theory (DFT) based physisorption studies of H ₂ on borophene in literature.	6
3.1	IVDW influence on different systems studied within the thesis work.	16
3.2	System size effects.	17
3.3	Input tags and parameters chosen for DFT calculations.	17
4.1	Formation energies (E_f) of vacancy in borophene.	21
4.2	Charge and distances in systems containing single vacancy and double vacancies.	24
4.3	Binding energies of adatoms tested.	25
4.4	Analysis on metal decorated systems.	26
4.5	Adsorption energies of second metal atom on single decorated borophene systems.	28
4.6	Analysis on double metal decorated systems.	28
4.7	Range of energies for pristine, SV and DV configurations in eV.	30

Chapter 1

Introduction

“That’s one small step for [a] man, one giant leap for mankind.” These words of Neil Armstrong after the successful landing of the lunar module of Apollo 11 spaceflight, inspired generations of engineers and scientists to dream big. Among the many state-of-the-art technologies used for this mission, the role hydrogen played, is worth mentioning. Hydrogen was used as a fuel for the second and third stages of the rocket launch. The electricity requirements of the modules was met by fuel cells which combined hydrogen and oxygen molecules to produce electricity. Water which was a byproduct of this reaction was used in the cooling system of some devices and for drinking purposes [1]. This was in the year 1969. Today, fossil fuels meet a good percentage of the energy demands of the growing world economy. This comes at the cost of pollution and global warming which makes its presence felt via natural disasters and climate changes. Hydrogen fuel has the potential to replace fossil fuels and fulfill the energy demands of the "energy-hungry" global society. However, even after half a century of research and development, hydrogen fuel, has not gained enough access to the market [2].

The lack of a viable option for hydrogen storage is one of the reasons why hydrogen technology has not reached its full potential [4]. Hydrogen can be produced from natural gas via steam methane reforming. With the help of carbon capture and storage technology, the CO₂ which is a byproduct, is captured and stored. Hydrogen produced in such a process is termed blue hydrogen. Hydrogen can also be produced from electrolysis, which is the splitting of water with the help of electricity to produce H₂ and O₂. The electricity required for this process can be generated from renewable energy sources such as solar and wind energy. Hydrogen produced via electrolysis, powered by renewable energy, is termed green hydrogen [3]. To be cost-effective, hydrogen in most cases is produced in large quantities in a centrally located production facility. Hydrogen is then transported to the point of end-use with the help of pipelines and trucks [5]. Storage of hydrogen within these transportation trucks and the end-use points requires storage technologies. The current technologies available need either extreme operating conditions or have poor efficiency and life cycle.

Some of the important parameters that are used to measure the utility of the storage technology are:

1. Gravimetric density (*GD*): Ratio of the weight of stored hydrogen in the system to the total weight of the system (which includes the weight of hydrogen as well). It is expressed in wt%.

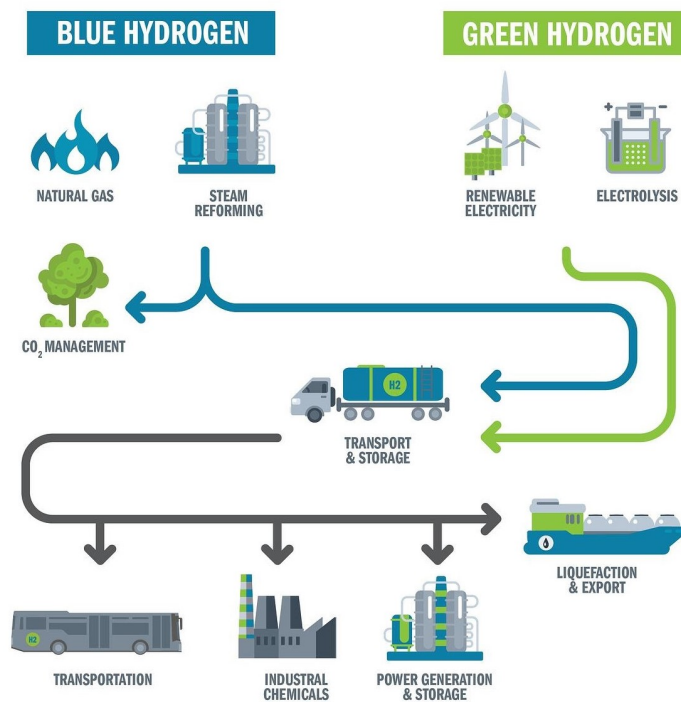


FIGURE 1.1: Production and storage methods of hydrogen [3].

2. Volumetric density (VD): Ratio of the weight of the stored hydrogen to the total volume of the system. It is expressed in $\text{g}(\text{H}_2)/\text{L}$.
3. Operating conditions: Temperature and pressure range at which the adsorption and desorption takes place in the system.
4. Cycle life: Number of adsorption and desorption cycles which the system can support.
5. Adsorption energy: Is related to the energy of interaction between the adsorbent and the H_2 molecule.

1.1 Outline of report

The report begins with a study of the existing hydrogen storage technologies in terms of the above-mentioned parameters in Chapter 2. This chapter also includes the research questions and the approach taken for the study. Chapter 3 presents the methods that were used and the arguments as to why certain techniques and tags were preferred over others. Discussion on the analysis of the results are presented in Chapter 4. Chapter 5 includes the conclusions and Chapter 6, the recommendations for further research.

Chapter 2

Scientific background

2.1 Existing technologies for hydrogen storage

In this section, the available methods for hydrogen storage will be discussed in terms of the mechanism of the hydrogen storage, its gravimetric and volumetric density, operating conditions and lifetime.

The physical-based hydrogen storage technologies are the more established methods available in the market. Among the physical-based technologies, the compressed and cryogenic technologies are the more advanced ones. Compressed hydrogen gas uses tanks that are not prone to hydrogen

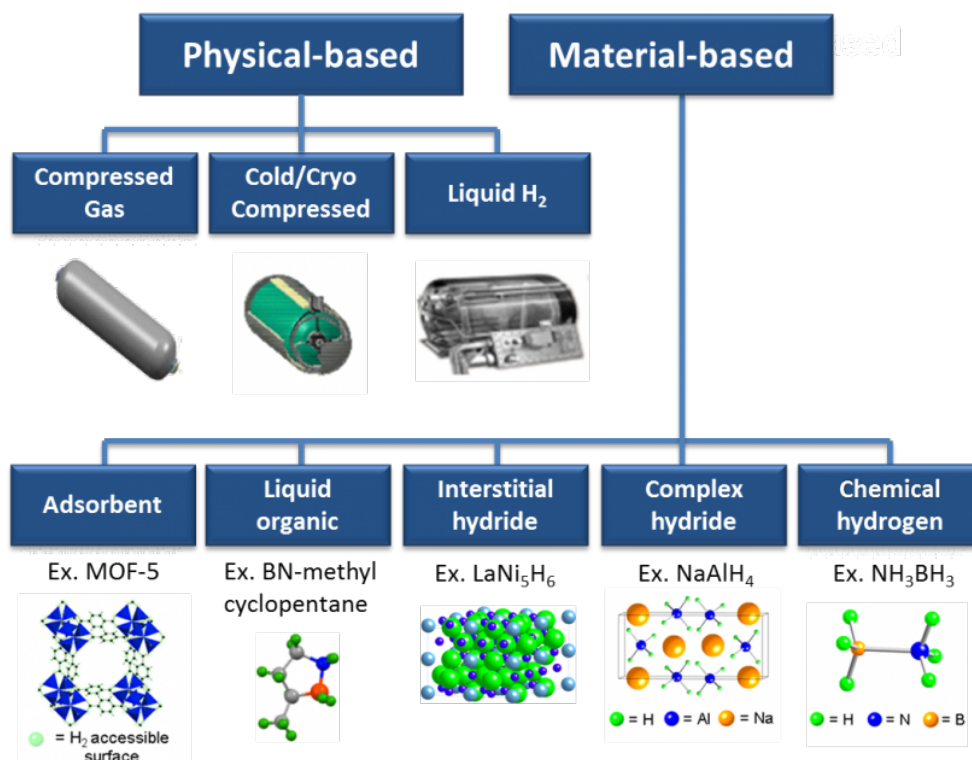


FIGURE 2.1: Available hydrogen storage methods [6].

embrittlement such as carbon fibre reinforced plastic and they exhibit a *GD* of 6.9 wt% and a *VD* of 18.6 g/L. The operating pressure is between 350 bar and 700 bar and a cycle life of 5500 is expected from this system. Even though compressed gas shows high *GD* and a good cycle life, it exhibits poor *VD* and

high cost [7]. Joule-Thomson coefficient (μ) is the ratio of change in temperature to the change in pressure at constant enthalpy. A positive μ indicates a drop in temperature with decreasing pressure while a negative μ indicates an increase in temperature with decreasing pressure. As seen in Figure 2.2, hydrogen has a negative Joule-Thomson coefficient in the operating conditions mentioned. Heat is produced during the isenthalpic expansion process of filling hydrogen from high pressure to low pressure [8]. Cryogenic tech-

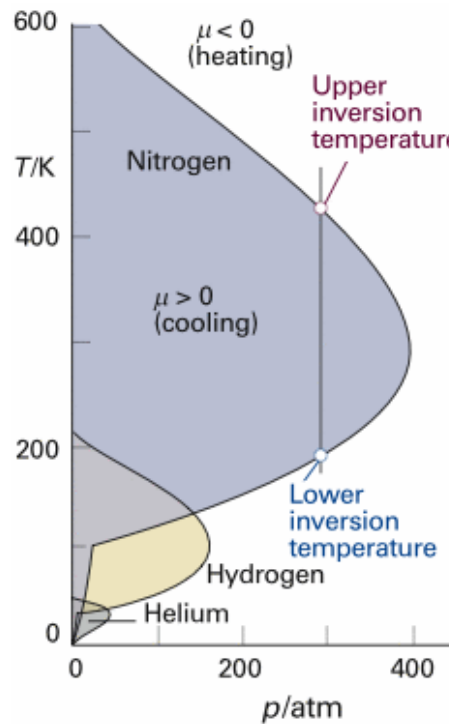


FIGURE 2.2: Joule-Thomson coefficient of H, He and N [9].

nology stores hydrogen at 21 K and offers a *GD* and *VD* of 7.5 - 20 wt% and 65 - 75 g/L respectively. High *GD* and *VD* of cryogenic systems are an advantage. However, cryogenic technology suffers from boiling off of the fuel from the tank due to the low heat of evaporation (0.44 kJ/mol) and specific heat (14 J/mol K) of hydrogen [4].

In material based methods, the hydrogen atoms are stored via the interaction between the H_2 molecule and the elements in the host materials. In metal hydrides, the metal or the alloy interacts with the H_2 molecule forming a metal hydride. The adsorption of H_2 is an exothermic process while the desorption is an endothermic process. Important examples of metal hydrides used for hydrogen storage include $LaNi_5$ and Mg. $LaNi_5$ has a high *VD* but a low *GD* and cycle life. Mg has a high *GD* and *VD* but suffers from poor dissociation kinetics [4].

In complex metal hydrides, the hydrogen atoms occupy the corners of the tetrahedron with atoms like N, B or Al at the centre. The H atoms bond with the atoms in the centre via covalent bonds. The negative charge of the polyatomic ion is balanced by the addition of a cation such as Li, Na, K or Mg. Some important complex metal hydrides are $NaAlH_4$, $LiBH_4$ and Mg_2NiH_4 .

The biggest disadvantage for NaAlH_4 is the poor thermodynamics and kinetics of hydrogen desorption. LiBH_4 suffers from poor kinetics of the desorption reaction while Mg_2NiH_4 exhibits both poor GD and desorption kinetics [4].

Metal-organic frameworks (MOFs) are porous structures that consist of metal ions connected to organic ligands. The interest in MOFs for hydrogen storage is due to the large free volumes, high surface area, low weight and tunable functionalities of MOFs. However, due to the low adsorption energy of H_2 and the presence of heavy metal dopants, there are issues such as low GD and VD that hampers the hydrogen storing ability of MOFs [10], [11].

2.2 2D materials

It can be seen from the above discussion that the established technologies have disadvantages and shortcomings that stand as hindrances to the market penetration of hydrogen fuel. The combination of two technologies that can complement each other in its functioning comes across as an excellent option to overcome some of the disadvantages of the individual technologies mentioned earlier. In this regard, 2D materials offer a good case to be considered for hydrogen storage due to their high surface area, low weight, high Young's modulus and strength. This is the reason why 2D materials such as graphene [12], [13], [14], [15], phosphorene [16], [17] and silicene [18], [19] were investigated for their hydrogen storage properties.

In this study, borophene is considered as a material that can aid the existing technologies. This is because boron is one of the lightest elements that can form repeated covalent bond structures which leads to a low weight of the system. Along with this, borophene provides large spaces for hydrogen adsorption and has good mechanical properties [20].

2.2.1 Borophene structures

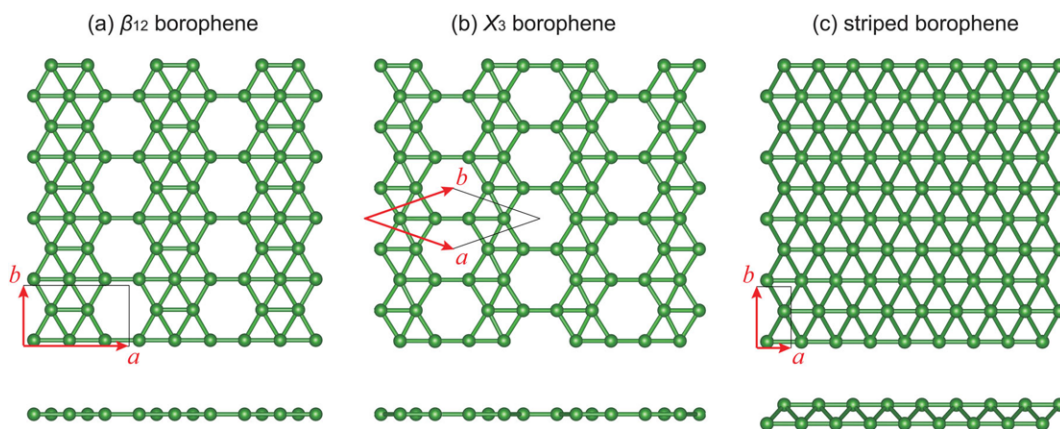


FIGURE 2.3: Commonly studied borophene structures- (a) β_{12} , (b) χ_3 and (c) $2-Pmmn$ (striped) borophene [21].

The commonly studied borophene structures are 2- $Pmmn$ (also known as striped borophene), β_{12} and χ_3 , as shown in Figure 2.3. 2- $Pmmn$ has a corrugated structure with a buckling height of 0.91 Å. Due to this structure, it has anisotropic mechanical and electronic properties. β_{12} and χ_3 are planar structures differing in boron vacancy distribution [22].

2.3 Physisorption on borophene

Physisorption studies of H_2 on borophene show that pristine borophene weakly interacts with the H_2 molecules. The binding energy of H_2 on pristine borophene was found to be in the range of -0.032 to -0.045 eV/ H_2 . A binding energy of -0.69 and -0.063 eV/ H_2 was found for double and single vacancy borophene respectively [23].

Inclusion of adatom has shown good potential in enhancing the binding energy of H_2 on borophene. The addition of the decorating atoms induces polarization of the H_2 molecule, thereby strengthening the interaction with the borophene substrate. Decorating metal atoms on both sides of the substrate show a higher hydrogen storage capacity than single decoration [23], [24]. Among the studies found in the literature for physisorption of H_2 on borophene, Li [24] and Ti [25] decorated borophene substrates are the best performers in terms of GD . They can reach up to 13.7 and 15 wt% respectively which can be seen from Table 2.1.

TABLE 2.1: Density Functional Theory (DFT) based physisorption studies of H_2 on borophene in literature.

Adatom	GD (wt%)	E_{ads} (eV/ H_2)
Li [24]	13.7	0.14
N [26]	6.22	0.14
Ti [25]	15	0.2
Ca [27]	9.5	0.24

An important point to be noted is that these values are calculated with *ab-initio* DFT calculations at 0 K. As temperatures increases, the GD also decreases as the interaction between the metal and the H_2 molecule gets weaker leading to less polarization of the H_2 molecule which was one of the factors that aided the interaction between H_2 and borophene [24]. Thus, physisorbed hydrogen molecules at higher temperatures can have enough energy to overcome the energy barriers leading to desorption.

2.4 Simulation studies on chemisorption

In literature, most of the studies on hydrogen storage in borophene are performed with H_2 adsorbed on borophene via weak van der Waals interactions [23], [24], [26]. In this thesis work, the possibility of using 2D materials

such as borophene to aid the established technologies in hydrogen storage is studied. One avenue identified is the utilization of the excess heat released during the storage processes of some of the above mentioned methods. Physisorption of H_2 on borophene as seen earlier, shows decreasing GD values with increasing temperatures. Chemisorption, on the other hand, can use the excess heat as it requires energy to overcome the activation barrier for hydrogen bond dissociation. The chemisorbed state is also more stable than the physisorbed state as the H atoms are bonded with B atoms via stronger covalent bonds.

While studies have been conducted on the synthesis and physical properties of borophane [28], [29], which is hydrogenated borophene, the scope of using chemisorbed hydrogen on borophene as a hydrogen storage method has not been studied extensively. As several factors can affect the chemisorption reaction such as the temperature, defects and adatoms present in the system, pressure, simulation studies are a good option as it provides more control over the parameters that can be adjusted. Simulation studies are less expensive than experimental studies and provide an excellent platform for high-throughput calculations. They also have the added advantage of being flexible and suitable to adjust to restrictions imposed due to global pandemics like SARS-CoV-2.

2.5 Research questions

As seen from the earlier discussions, H_2 chemisorption on borophene as a hydrogen storage method has not been studied extensively. The activation barrier height ($E_{ads-bar}$) which is the minimum amount of energy required to facilitate the chemisorption reaction must be examined. The energy difference between the initial physisorbed state and the final chemisorbed state (ΔH_{ads}) which along with $E_{ads-bar}$ determines the barrier height for desorption reaction ($E_{des-bar}$) are important parameters that need to be investigated. From the literature, it was seen that defective borophene and metal decorations on pristine borophene enhance the adsorption energy of H_2 on the substrate. Additionally, spillover mechanism which is the dissociation of H_2 molecules adsorbed on metal catalysts [30], provides further motivation to investigate metal decorations. Thus, analysis must be done to examine the effect of defects and metal decorations on $E_{ads-bar}$ and ΔH_{ads} .

The research objectives of the thesis are outlined below:

1. To compare the properties of H_2 physisorption and chemisorption on different borophene systems.
2. To ascertain the $E_{ads-bar}$ and ΔH_{ads} which determines the $E_{des-bar}$ for H_2 molecule on pristine and defective borophene.
3. To examine the influence of metal decorations on the $E_{des-bar}$ of pristine borophene.

Chapter 3

Methodology

In this chapter, the methods and techniques used for the simulation studies are discussed briefly. This chapter consists of sections on density functional (DFT), nudged elastic band method (NEB), discussion on the files used and sensitivity analysis to determine the tags used in the files.

3.1 Density functional theory

3.1.1 Overview

Attempts to model the multi-electron system were started in the early 20th century such as the Hartree-Fock (HF) [31], Thomas-Fermi (TF) [32], Thomas-Fermi-Dirac (TFD) [33] models. But TF and TFD models could not take into account the quantum mechanical nature of electrons completely leading to errors when compared with experimental data. Models such as HF worked with the wave functions leading to calculations in $3n$ dimensions for a system with n electrons [34]. Density functional theory (DFT) overcame these issues to become one of the most popular quantum mechanical multi-electron modelling methods, if not the most [35].

DFT is founded on two theorems:

Theorem 1 states that at a given external potential, the total energy of a system of electrons is a functional of the electron density. This allows one to work with the electron density, which is an entity in 3 dimensions, and to find the ground state energy of the system. This is a big reduction in terms of number of dimensions compared to previous models which attempted to find the ground state energy state via the wavefunctions which leads to a $3n$ dimensional model for n electrons.

Theorem 2 states that the electron density that minimizes the total energy is the ground-state electron density and this electron density can be found by the variational principle [36].

3.1.2 Kohn-Sham approach

Earlier attempts such as the TF model and the TFD model did not take into account the shell structure of the electrons around the nucleus of the atom. This led to a poor representation of the electronic kinetic energy term. Kohn

Sham (KS) approach avoided this problem by constructing fictitious one-electron orbitals for the N-electron system. Thus, solving the Schrödinger equation for the multielectron system became simplified and the shell structures of the atoms were reflected in the solutions [37].

Energy Terms

The energy functional which is to be minimized to find the ground state energy can be divided into four parts according to the KS approach. These parts are kinetic energy, external energy, hartree energy and exchange-correlation energy.

1. Kinetic energy ($E_{\text{kin}}^{\text{non}}$): In the KS approach, the non-interacting electrons were given fictitious one-electron orbitals as mentioned earlier and the kinetic energy is given by

$$E_{\text{kin}}^{\text{non}} = -\frac{1}{2} \sum_{n=1}^{\infty} \phi_i^*(\mathbf{r}) \nabla^2 \phi_i(\mathbf{r}) \quad (3.1)$$

Note that ϕ is the fictitious KS-orbital. Since the kinetic energy is treated with one-electron orbitals, the kinetic energy for the non-interacting part is calculated accurately while the quantum mechanical interaction part of the electrons is treated in the exchange-correlation part.

2. External energy (E_{ext}): The Coulombic attraction between an electron and nuclei is referred to as the external potential $U_{\text{ext}}(\mathbf{r})$ and the expectation value of $U_{\text{ext}}(\mathbf{r})$ over the entire volume space gives the external energy.

$$E_{\text{ext}} = \int U_{\text{ext}}(\mathbf{r}) \rho(\mathbf{r}) d\mathbf{r} \quad (3.2)$$

Here, ρ is the electron density at a point \mathbf{r} in space.

3. Hartree energy (E_H): The electron-electron repulsive energy in a non-interacting system is referred to as the Hartree energy. It is calculated as the interaction between electron at \mathbf{r} and the mean electron density at \mathbf{r}' and is given by

$$E_H[\rho(\mathbf{r})] = \int U_H(\mathbf{r}) \rho(\mathbf{r}) d\mathbf{r} = \frac{1}{2} \iint \frac{\rho(\mathbf{r}) \rho(\mathbf{r}')}{|\mathbf{r} - \mathbf{r}'|} d\mathbf{r} d\mathbf{r}' \quad (3.3)$$

where U_H is the Hartree potential.

4. Exchange-Correlation energy (E_{xc}): The quantum effects which are not taken into account in the previous three energy terms are included in the exchange-correlation energy term. Exchange energy stems from the Pauli's exclusion principle which states that two electrons cannot have the same four quantum numbers. This results in less overlap of the electron orbitals with the same spin and thus less repulsion energy. Correlation energy term arises when two electrons with different spins are correlated due to their Coulombic repulsion energy [38].

The contribution of each of the energy term discussed above for an He atom is shown in Figure 3.1.

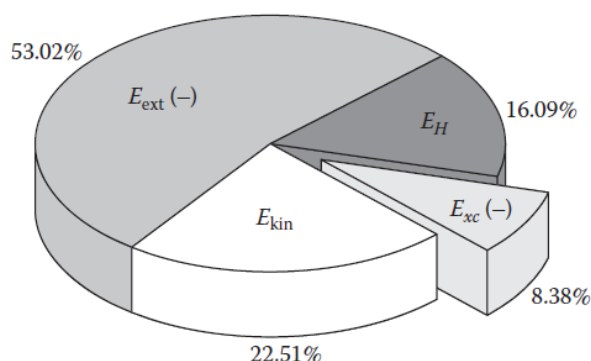


FIGURE 3.1: Contributions of the energy terms for an He atom [38].

Exchange-Correlation functionals

Several models for the exchange correlation approach are available with two commonly known approaches being Local-density approximation (LDA) and Generalized gradient approximation (GGA). In LDA, the volume space of the system is divided into smaller sections and it is assumed that electron density in that section is uniform. However, since the actual systems do not have uniform electron density, this approach is found lacking in the following aspects:

1. LDA overestimates the cohesive energy and underestimates the lattice parameters.
2. Adsorption energies are overestimated.
3. It is not suitable for systems with weak bonds and van der Waals attraction [38].

GGA incorporates both the local electron density as well as the density gradient to better capture the varying electron density picture in real systems. The Perdew–Burke–Ernzerhof (PBE)-GGA functional which is used in this study is a highly popular functional [39]. However, the GGA approach is not without drawbacks:

1. Calculations with GGA predict approximately 50% smaller band gaps [40].
2. There is an inherent error in GGA bond length calculations [38].

Pseudopotential

The potential of the electrons that are involved in the energy terms discussed above is written in the form of pseudopotentials (PP). The major steps are freezing the core electrons and pseudizing the wave function of the valence electrons. Freezing the core electrons is done because the core electrons do not involve much during the chemical reactions that take place in most cases. Thus, freezing the core electrons means assuming the core electrons are frozen and dealing only with the valence electrons. This is done so as to decrease the computational load. The wave function of the valence electrons can pass through the core electrons region. Due to the Pauli's exclusion principle, the orbitals have to be orthogonal to each other (to make $\phi^* \phi = 0$). This leads to rapid oscillations of the valence electron wave functions in this region as it increases the computational load. Psuedizing the wave function means replacing the rapidly oscillating function with a featureless curve thus avoiding the nodes. Depending on the pseudizing procedure the pseudopotentials are classified as Norm-conserving PPs, Ultrasoft PPs and Projector augmented wave (PAW) potentials. In this study, the PAW potentials are used as they are able to reproduce the information about the core region quite well leading to an overall increase in accuracy.

Solving Kohn-Sham equations

The main objective of the model is to arrive at the ground state energy level and derive the corresponding physical properties. Solving the Kohn-Sham equation to obtain the ground-state electron density is done iteratively. Initially, an electron density is defined and then the equations are solved iteratively and once the convergence criteria are met, the iterations are stopped. In Figure 3.2, H_{KS} is the Hamiltonian obtained from the energy terms discussed above. ϵ_i is the eigenvalue of wavefunction ϕ_i . Once the electronic ground state is found from the iterations, the forces on the ions and the position of the ions can be calculated. From the electronic ground state, the hamiltonian (\hat{H}) is known and from the electronic density, the electronic wave functions (ϕ) are known. The force acting on the ions is given by:

$$F_I = - \langle \phi_i | \frac{\partial \hat{H}}{\partial r_I} | \phi_i \rangle \quad (3.4)$$

Once the forces acting on the ions reach convergence, the energy and the other properties are determined.

The reason why we are allowed to treat the nuclei and the electrons separately is because of the Born-Oppenheimer approximation. This approximation allows the nuclei and electrons to be treated separately because the nuclei are much heavier than the electrons and electrons respond faster to the changes in surroundings compared to the nuclei [38].

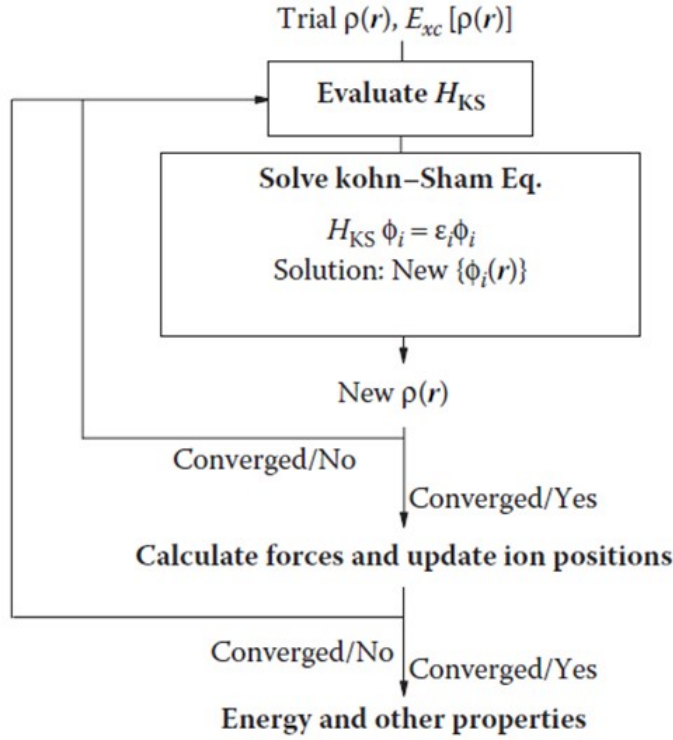


FIGURE 3.2: Flowchart for solving KS equations [38].

3.2 Nudged elastic band method

Nudged Elastic Band (NEB) method is used to find the Minimum Energy Pathway (MEP) between two relaxed states. NEB starts with connecting the two states with an initial linear pathway with the number of images set in the calculation. This pathway connecting the images is called a band. The images in the band are then nudged along the band to attain zero force configurations. The reason why we are targeting zero force is that force is the first derivative of energy and zero force means a local minimum of the energy. The nudging is constrained by fictitious spring forces added between the images to ensure that the band is continuous. The forces that are minimized to attain the MEP are the projection of the spring forces along the band and the projection of the interatomic forces, within the images, perpendicular to the band. After each nudging, electronic minimization via DFT is done to calculate the forces for the next direction of nudging. Once all the images along the band reach the convergence specified by the convergence criteria, the band connecting the images becomes the MEP. To make sure that the highest energy image is at the saddle point, the climbing image method is followed. Here, the tangential force of the image with the highest energy is reversed forcing the image to climb up the band [41], [38].

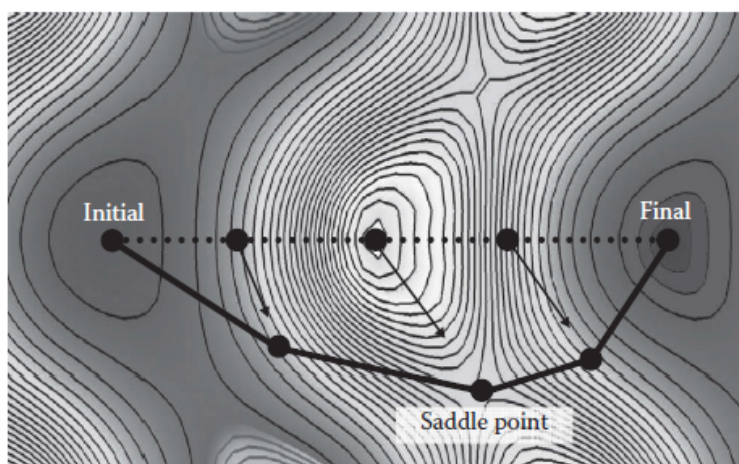


FIGURE 3.3: Potential energy landscape of the reaction whose initial, intermediary and final states are shown [38].

3.3 Vienna ab initio simulation package

Vienna ab initio simulation package (VASP) is a package for doing *ab-initio* quantum mechanical simulations. VASP is used for computing approximate solutions to the Schrödinger equation in many-body systems [42]. In this thesis work, the VASP package is used to perform the DFT calculations.

3.3.1 Input files

The input files needed for DFT calculations in VASP are:

1. INCAR: This file contains the tags that determine how the calculations will run. More discussion on the tags used will be in the following sections.
2. KPOINTS: A file that contains the k-points used in the calculations.
3. POSCAR: contains information on the size of the unit cell/supercell used, the number of atoms per element in the calculations and the positions of the atoms in the supercell.
4. POTCAR: contains the pseudopotential, which was discussed earlier, for each element. The ordering of the pseudopotentials of the atoms in the POTCAR file must follow the order prescribed in the POSCAR file.

3.4 Input tags

This section contains a brief discussion on the input tags used in the input files and sensitivity analysis done to determine the value of the tags.

3.4.1 KPOINTS

The calculations done in this study, involve wave functions of electrons and one mole of a substance contains around 10^{23} atoms making it unfeasible to do the calculations in the real space. Since there is periodicity in the arrangement of the atoms in the solids we are interested in, one can make use of the reciprocal lattice vector G . In the case of electrons, since they are represented by the wave vector, k , one can work with the KS equations in the reciprocal space. Bloch theorem and Fourier theorem provides the framework to make this transition from the real space to the reciprocal space.

Bloch theorem treats the influence of the periodic potential of the nuclei on the valence electrons as a perturbation by mapping the plane wave function of the valence electrons onto the periodic pattern of the nuclei of the atoms in the solid.

$$\psi_k(\mathbf{r}) = u_k(\mathbf{r})\exp(i\mathbf{k} \cdot \mathbf{r}) \quad (3.5)$$

In Equation. 3.5, $u_k(\mathbf{r})$ is a function with the same periodicity as that of the potential of the nuclei.

According to the Fourier theorem, a function that is periodic within two limits in the real space can be expressed as the weighted sum of the harmonically related sinusoids. Since $u_k(\mathbf{r})$ is periodic within the Wigner-Seitz cell, one can express $u_k(\mathbf{r})$ as

$$u_k(\mathbf{r}) = \sum_G c_k(G)\exp(i\mathbf{G} \cdot \mathbf{r}) \quad (3.6)$$

where $c_k(G)$ is the Fourier expansion coefficient. Combining Equation 3.5 and Equation 3.6, we get

$$\psi_k(\mathbf{r}) = \sum_G c_k(G)\exp(i(\mathbf{k} + \mathbf{G}) \cdot \mathbf{r}) \quad (3.7)$$

Thus, with the help of Equation 3.7, the calculations involving the electrons can be done with the help of k-points and reciprocal lattice vector in the reciprocal space. Owing to the periodic nature of the reciprocal lattice, only a few number of k-points found in the irreducible brillouin zone is required, thus reducing the computational load of the simulations [38]. The convergence of the KPOINTS used in shown in Figure E.6.

3.4.2 ENCUT

The kinetic energy of the plane waves is proportional to $|\mathbf{G} + \mathbf{k}|^2$ where G represents the reciprocal lattice vector and k corresponds to the wave vector. Since the aim is to converge to the lowest energy level, the plane waves with energies larger than the cutoff energy level are excluded. Thus, only the plane waves that satisfy the condition

$$\frac{1}{2} |\mathbf{G} + \mathbf{k}|^2 \leq \text{ENCUT} \quad (3.8)$$

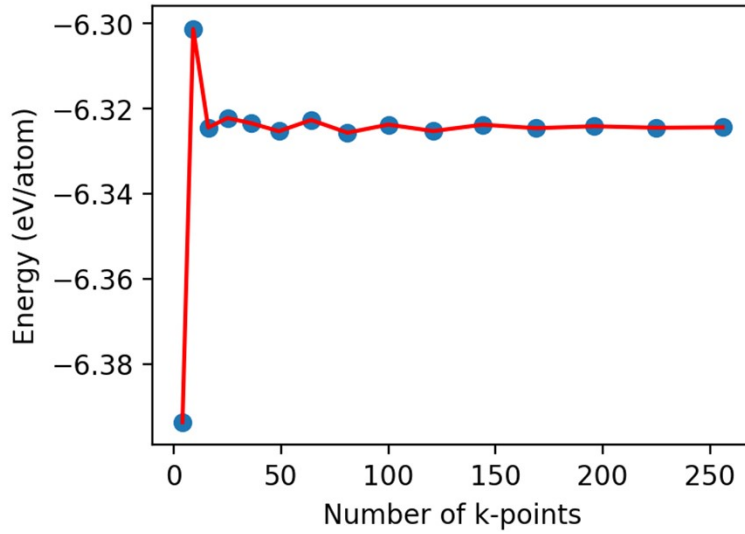


FIGURE 3.4: KPOINTS convergence of a 4×5 pristine borophene supercell with an ENCUT value of 500 eV.

are included. The convergence of the ENCUT used in shown in Figure 3.5.

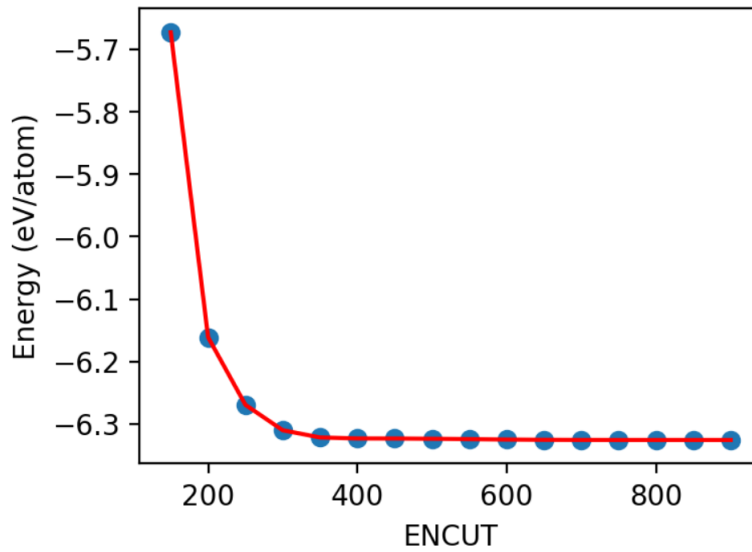


FIGURE 3.5: ENCUT convergence of a 4×5 pristine borophene supercell with KPOINTS of $5 \times 5 \times 1$.

ISMear

Borophene is metallic in nature. Charge densities do not decay smoothly around the Fermi gap for metals at 0 K. This causes a sharp drop in the occupancy causing issues in calculations around the Fermi level. Smearing makes the charge density function decay smoothly by introducing partial occupancies. Gaussian smearing is used for the calculations in the report as it performs better than Methfessel-Paxton 1 and 2 in terms of the minimum energy of the ground state as well as time taken for the calculations as shown in

Appendix D. Gaussian smearing introduces a delta-like function for the fictitious temperature around the Fermi level and the standard deviation around the Fermi level is determined by the sigma parameter.

3.4.3 IVDW

IVDW tag ensures van der Waals interactions are included in the energy calculations. In this study the DFT-D2 method of Grimme is used [43]. The energy difference between the initial physisorbed state and the final chemisorbed state (ΔH_{ads}) calculated with and without IVDW for different configurations tested are listed in Table 3.1.

TABLE 3.1: IVDW influence on different systems studied within the thesis work.

System	$(\Delta H_{\text{ads}})_{\text{IVDW}}$ [eV]	$(\Delta H_{\text{ads}})_{\text{without IVDW}}$ [eV]	% difference
Pristine	1.39	1.38	0.72
SV	1.53	1.44	5.88
DV	1.48	1.37	7.43
Li	1.22	1.05	13.93
Na	1.19	1.02	14.28
K	1.1	0.95	13.64
Ca	1.3	1.21	6.92

The percentage difference is calculated as following:

$$\frac{(\Delta H_{\text{ads}})_{\text{IVDW}} - (\Delta H_{\text{ads}})_{\text{without IVDW}}}{(\Delta H_{\text{ads}})_{\text{IVDW}}} \times 100 \quad (3.9)$$

It can be seen that the pristine borophene system has the least difference percentage. This might be because only the H_2 molecule is adsorbed with van der Waals interactions. However, this is not the case with metal decorations as the metal atoms interact with the substrate via van der Waals forces leading to a higher percentage difference in metal decorations compared to pristine and defective borophene.

3.4.4 System size effects

System size effect refers to the influence of the choice of the simulation box cell size on the obtained results. Small simulation box sizes will have interactions from the periodic images of the atoms. Larger box sizes thus lead to smaller system size effects. However, with the increase in the number of atoms in the simulation cell, there will be an increase in the computational load. Thus, there must be a balance between the computational time required for the calculations and the amount of system size effects in the final results. Three simulation box sizes with an interlayer spacing of 30 Å were picked to

study the system size effects in this work. The system sizes are chosen with respect to the conventional unit cell of the striped borophene. Their effects on the ΔH_{ads} values of two metal decorated systems are investigated and are presented in Table 3.2. The reason to chose Li and K is that Li and K are the

TABLE 3.2: System size effects.

System size	Number of atoms	$(\Delta H_{\text{ads}})_{\text{Li}}$ [eV]	$(\Delta H_{\text{ads}})_{\text{K}}$ [eV]
4×5	40	1.23	1.1
6×3	36	1.14	1.23
10×5	100	1.1	1.2

smallest and largest metal atoms in size respectively which were used in this study. It can be seen that there are system size effects in the calculations with the ΔH_{ads} values of 4×5 and 10×5 simulation boxes differing by up to 0.13 eV. However, a system size of 4×5 was chosen in this thesis work to validate the obtained results with existing literature results, where similar supercell dimensions were chosen [23], [24].

3.4.5 Input parameters

From the sensitivity analysis of the input tags and parameters mentioned in the above sections, the following values for the tags and parameters were chosen. In Table 3.3, EDIFF is the stopping criterion for relaxation of the

TABLE 3.3: Input tags and parameters chosen for DFT calculations.

Parameter/tags	Value
KPOINTS	5*5*1
ENCUT	500 eV
ISMEAR; SIGMA	0; 0.3
EDIFF	10E-6
EDIFFG	-0.001
IBRION	2
IVDW	1
Supercell dimension	4×5

electronic degrees of freedom and EDIFFG is the stopping criterion for ionic relaxation loop. IBRION tag determines the algorithm by which the ions are updated and moved. IBRION = 2 is the conjugate gradient algorithm which is usually recommended for poor initial guesses. IVDW= 1 uses the DFT-D2 method of Grimme to take into account the van der Waals interactions [43]. ISIF tag determines which degrees of freedom of the supercell are allowed to change. In this thesis work, ISIF = 4 is chosen which allows the change of the

positions of the ions and the change of the cell shape but not the cell volume so that no relaxation along the c-axis which is vacuum for monolayers, takes place. The supercell dimensions are chosen with respect to the conventional unit cell of the striped borophene. An interlayer spacing of 30 Å is chosen so as to avoid interactions between the periodic layers [42].

3.4.6 Energy profile and associated terms

Energy profile of a H_2 chemisorption reaction on a pristine borophene system and the associated terms are shown in Figure 3.6. ΔH_{ads} is the enthalpy of the adsorption reaction and indicates whether the reaction is spontaneous or not. $E_{\text{ads-bar}}$ is the activation barrier height of the adsorption reaction while $E_{\text{des-bar}}$ is the activation barrier height of the desorption reaction. Note that $E_{\text{des-bar}}$ is the sum of $E_{\text{ads-bar}}$ and $|\Delta H_{\text{ads}}|$.

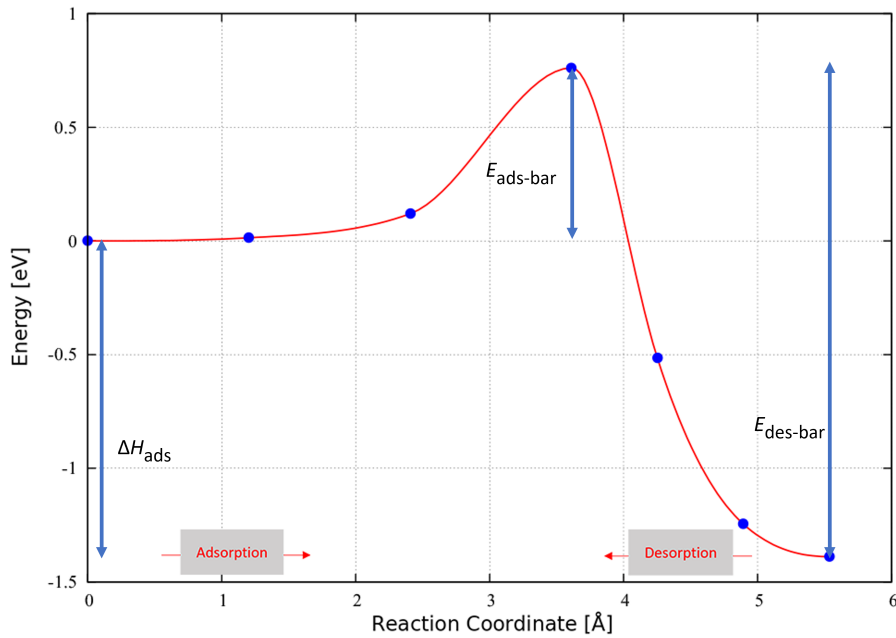


FIGURE 3.6: Energy profile of a chemisorption reaction on a pristine borophene system with the associated terms labeled.

Chapter 4

Results and Discussion

4.1 Pristine

To study the decomposition reaction of H_2 on pristine borophene, various non-equivalent physisorption/chemisorption sites on the borophene substrate were considered which are listed in Figure A.1 and Figure A.2 in Appendix A. The most stable H_2 physisorption and chemisorption configurations, i.e., the initial and final states respectively, are shown in the Figure 4.1. Adsorp-

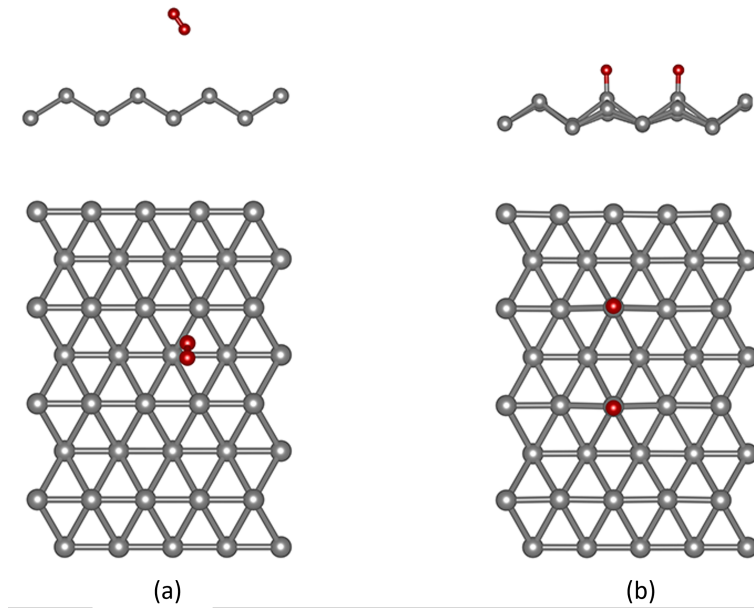


FIGURE 4.1: (a) Physisorbed and (b) chemisorbed states of H_2 on pristine borophene. Grey spheres represent B atoms while red spheres represent H atoms.

tion energy of H_2 molecule ($E_{ads}^{H_2}$) on a substrate is calculated as

$$E_{ads}^{H_2} = E_{\text{substrate}+H_2} - E_{\text{substrate}} - E_{H_2} \quad (4.1)$$

Here, $E_{\text{substrate}+H_2}$ and $E_{\text{substrate}}$ refer to the total energies of the system with H_2 adsorbed on it and that without the H_2 adsorbed respectively. E_{H_2} is the energy of a hydrogen molecule. $E_{ads}^{H_2}$ on pristine borophene was found to be $-0.02 \text{ eV}/H_2$ which is in close agreement with values found in literature [23].

The H atoms in the H_2 molecule are held together by electrostatic forces of attraction with the two H atoms having a charge $+0.029 e$ and $-0.02 e$ respectively making the total sum of charge within the H_2 molecule close to zero. Here, e is the charge of an electron and is equal to 1.6×10^{-19} C. The H-H bond length in the H_2 molecule is 0.75 \AA which is close to the H-H bond length of the free H_2 molecule. The distance between H_2 molecule and borophene substrate is found to be 3.6 \AA .

For the stable chemisorption configuration, there is a charge transfer of $0.45 e$ from the borophene substrate to the H atoms. Due to this enhanced interaction, the B-H bond length is 1.2 \AA which is in close agreement with the B-H bond length value found in earlier studies [29]. The two H atoms are separated by a distance of 3.01 \AA . Enthalpy of a hydrogen chemisorption reaction (ΔH_{ads}) is calculated as

$$\Delta H_{\text{ads}} = E_{\text{chem}} - E_{\text{phys}} \quad (4.2)$$

Here, E_{chem} and E_{phys} refer to the total energies of the chemisorbed and the physisorbed states of H_2 on borophene substrate respectively. On pristine borophene, ΔH_{ads} was found to be -1.39 eV . To study whether the reaction is kinetically favourable, the NEB method was implemented. The reaction pathway from the initial adsorbed state (IS) to the final dissociated state (FS) via the transition state (TS) is shown in the Figure 4.2. The total charge on the H_2 molecule increases from $0.01 e$ (IS) to $0.09 e$ (TS) and to $1 e$ (FS) with the H atoms in both the TS and FS being negatively charged. This leads to the increase in the H-H bond length from 0.75 \AA (IS) to 0.95 \AA (TS) and 3.01 \AA (FS) due to the increasing Coulomb repulsion between two negatively charged H atoms. The boron atoms interacting with the H_2 molecule becomes more positive by losing electrons to the H_2 molecule, going from $-0.001 e$ (IS) to $-0.19 e$ (TS) and $-0.83 e$ (FS) per boron atom. This leads to increased interaction between the borophene substrate and the H_2 molecule leading to a decrease in the distance between the H_2 molecule and borophene, from 3.6 \AA (IS) to 1.58 \AA (TS) and 1.2 \AA (FS).

Therefore from the above analysis, it is evident that the chemisorption of the hydrogen molecule is catalysed by the charge that is transferred from borophene to the H_2 molecule. From Figure 4.2, it is seen that the activation barrier for the reaction is 0.76 eV which is in agreement with previous studies [45] [29]. This indicates that even though hydrogen chemisorption onto borophene is thermodynamically favourable, the H_2 molecules must overcome a large activation barrier making the chemisorption reaction kinetically unfavourable.

4.2 Vacancies

As seen earlier in the case of pristine borophene, the chemisorption of H_2 molecule is facilitated by the charge transfer from borophene onto the H_2 molecule. Since striped borophene is metallic in nature, creating a vacancy

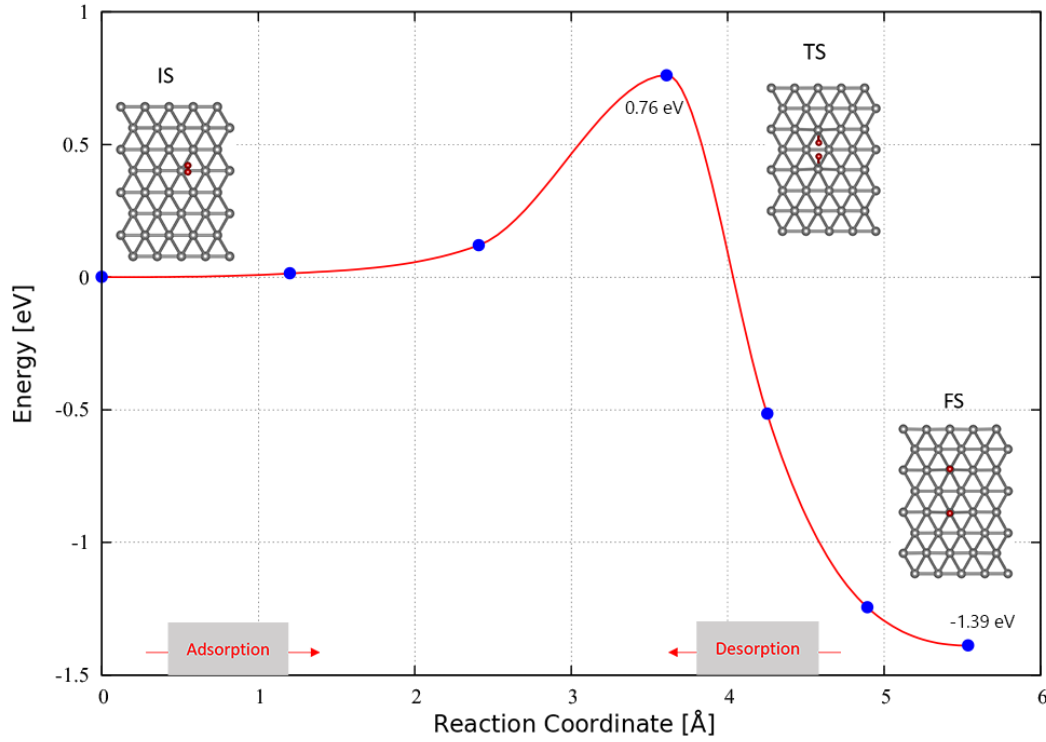


FIGURE 4.2: Minimum energy pathway corresponding to H_2 dissociation on pristine borophene. For the reaction, the ΔH_{ads} and $E_{\text{ads-bar}}$ was found to be -1.39 eV and 0.76 eV respectively. The blue dots are the NEB images while the red line connecting the blue dots is a guide to the eye. The NEB images in this report are generated from the scripts provided by the Henkelman group [44].

in the system will lead to the boron atoms surrounding the vacancy being more negatively charged. For the defective borophene, single vacancy (SV) and double vacancy (DV) borophene structures are studied within this work. Formation energy (E_f) of a vacancy in borophene is calculated as

$$E_f = E_{\text{defect}} - \frac{N - n}{N} E_{\text{pristine}} \quad (4.3)$$

Here, E_{defect} and E_{pristine} are the total energies of the defective and pristine borophene systems respectively. n is the number of B atoms removed and N is the total number of B atoms in the pristine system. The E_f of SV and DV are listed in Table 4.1.

TABLE 4.1: Formation energies (E_f) of vacancy in borophene.

Vacancy type	Calculated E_f [eV]	Literature E_f [eV]
SV	0.01	0.12 [23]
DV	1.18	1.3 [23]

The discrepancies in the calculated and the literature values can be attributed to the different INCAR tags used, different supercell dimensions and a different package used for the *ab-initio* DFT calculations.

Various non-equivalent positions for the physisorption and chemisorption sites on the vacancy were investigated which are listed in Figure A.3 and Figure A.4 respectively for single vacancy system and Figure A.5 and Figure A.6 respectively for double vacancy system in Appendix A. The most stable H₂ physisorption and chemisorption configurations are shown in the Figure 4.3 and Figure 4.4 for single vacancy and double vacancies respectively. The dissociated state of H near the vacancy is more stable than the

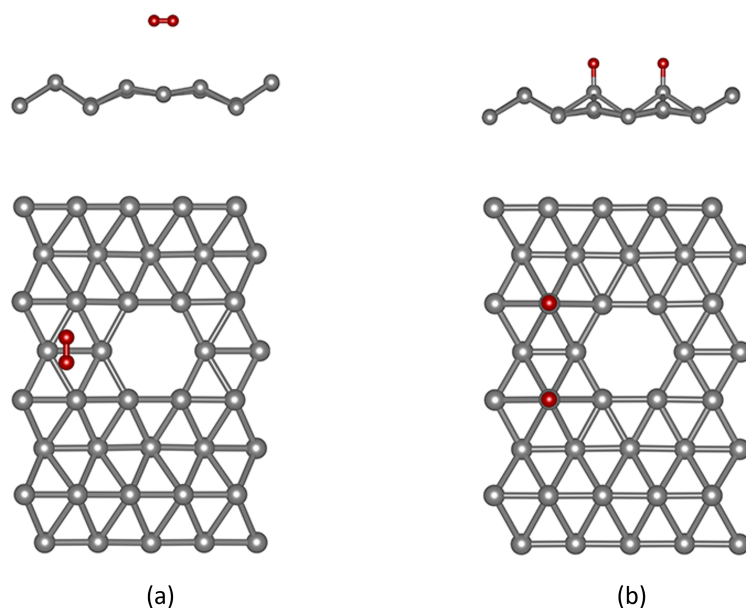


FIGURE 4.3: (a) Physisorbed and (b) chemisorbed states of H₂ on single vacancy borophene.

physisorbed state. The chemisorption reaction of the H₂ molecule in SV and DV is exothermic by 1.53 eV and 1.48 eV making the chemisorption reactions on these structures thermodynamically favourable.

NEB method was performed to study the activation barrier of the dissociation reaction for single and double vacancies (Figure 4.5 and Figure 4.6). Similar to the mechanism seen in pristine borophene, the H-H bonds in H₂ break due to the addition of charges on the H atoms, making them more negative and thus increasing the Coulombic repulsion between them. The charge on H, the distance between borophene and H₂ molecule (D_{H-B}) and the H-H bond length (D_{H-H}) are listed in the Table 4.2. Note that the charge on H in Table 4.2 is the average charge on the two H atoms.

As expected, D_{H-B} decreases and D_{H-H} increases from the initial state (IS) to the final state (FS) as more charge is transferred from borophene to the H₂ molecule along the adsorption pathway. The activation barriers for the chemisorption reaction for SV and DV are found to be 0.69 eV and 0.62 eV respectively which are lower than the activation barrier for H₂ dissociation in the pristine borophene system.

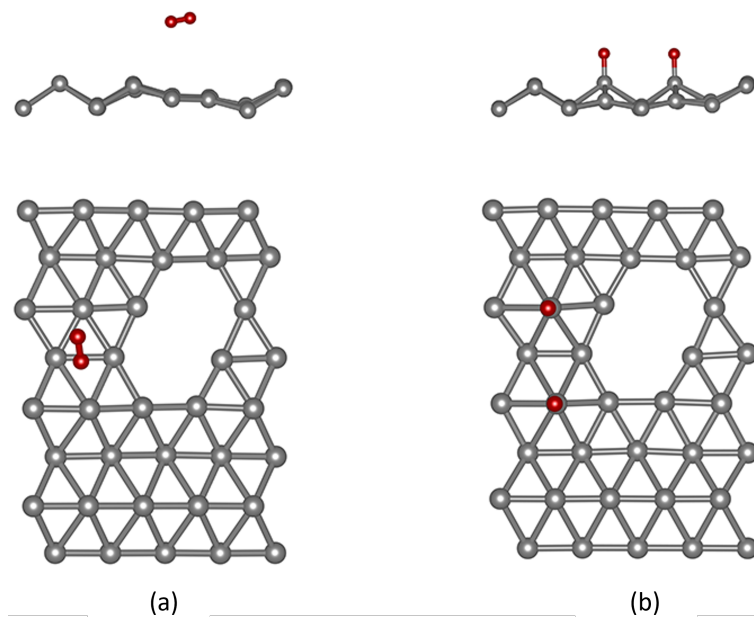


FIGURE 4.4: (a) Physisorbed and (b) chemisorbed states of H_2 on double vacancy borophene.

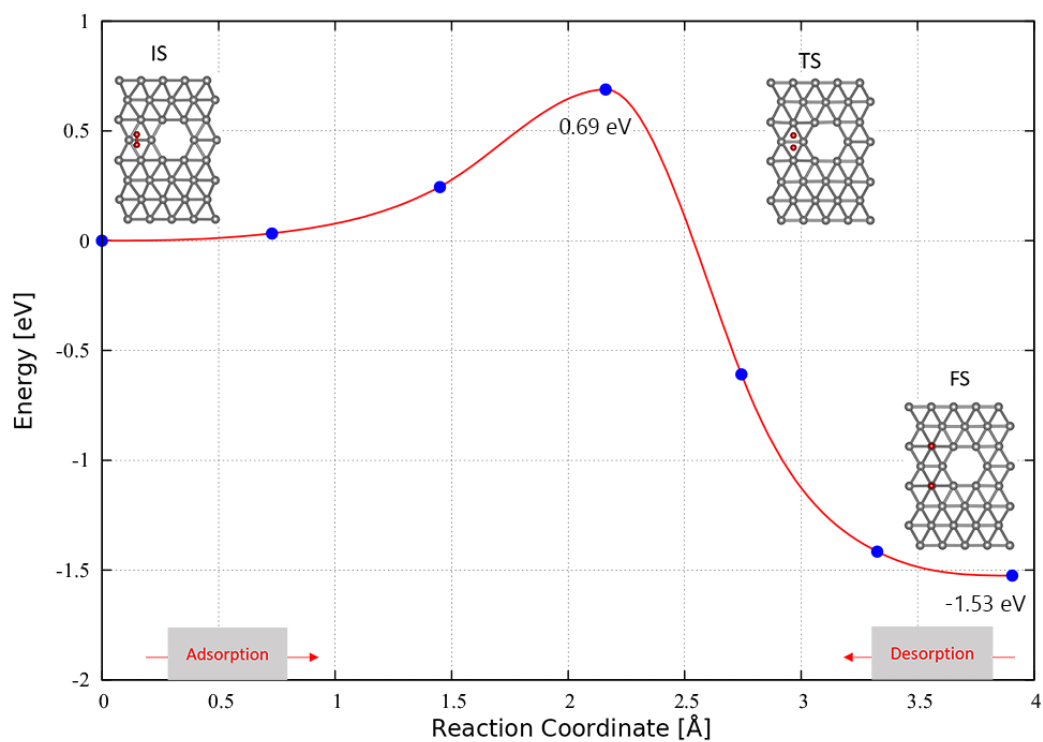


FIGURE 4.5: Minimum energy pathway corresponding to H_2 dissociation on single vacancy borophene. For the reaction, the ΔH_{ads} and $E_{\text{ads-bar}}$ was found to be -1.53 eV and 0.69 eV respectively.

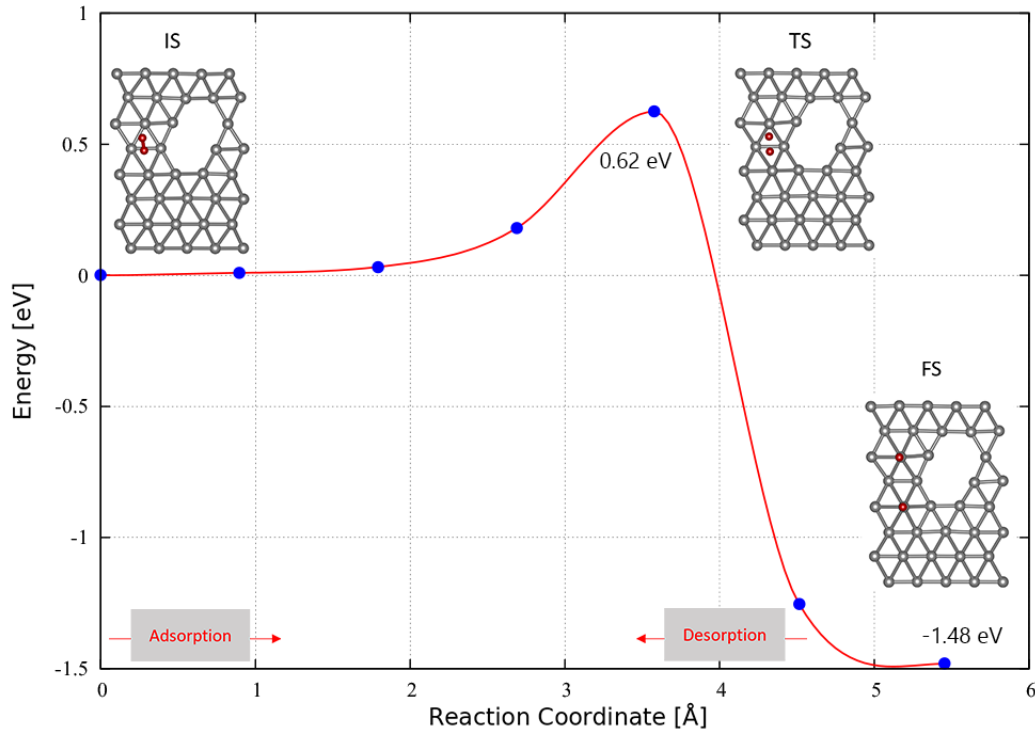


FIGURE 4.6: Minimum energy pathway corresponding to H₂ dissociation on double vacancy borophene. For the reaction, the ΔH_{ads} and $E_{\text{ads-bar}}$ was found to be -1.48 eV and 0.62 eV respectively.

TABLE 4.2: Charge and distances in systems containing single vacancy and double vacancies.

System	Charge on H [e]	$D_{\text{H-B}}$ [Å]	$D_{\text{H-H}}$ [Å]
SV _{IS}	0.01	2.96	0.75
SV _{FS}	0.5	1.2	2.9
DV _{IS}	0.01	2.99	0.75
DV _{FS}	0.5	1.2	2.86

4.3 Metal decoration

To reduce $E_{\text{ads-bar}}$ and the magnitude of ΔH_{ads} , metal decorations were used within this study. To examine whether the decorating atoms will form clusters in the system, the binding energies of the decorating atoms were calculated. Binding energy of a metal on borophene substrate (E_{b}^{M}) is defined as

$$E_{\text{b}}^{\text{M}} = E_{\text{substrate+M}} - E_{\text{substrate}} - E_{\text{M}} \quad (4.4)$$

where, $E_{\text{substrate+M}}$, $E_{\text{substrate}}$ and E_{M} refer to the total energies of substrate with metal atom, substrate without metal atom and of a single metal atom.

If the binding energy is negative, it can be established that the decorating atoms would not form clusters in the system as the interaction between the metal atom and the substrate is stronger than the metal-metal interactions. As can be seen from Table 4.3, the atoms that did not cluster are Li, Na, K, Ca

TABLE 4.3: Binding energies of adatoms tested.

Element	E_b^M [eV]
Li	-1.485
Na	-1.53
K	-2.01
Ca	-1.805
Mg	-0.218
N	0.618
Be	0.734
Ti	0.35

and Mg. Since the binding energy of Mg is close to zero, Mg was not used as a decorating atom. The atoms that were selected were alkali metals while Ca is the only metal that is not a Group 1 metal.

The physisorbed and the chemisorbed configurations that were chosen for the study for the metal decorations are shown in the Figure 4.7. It must be noted that Figure 4.7 shows the configurations for K decorated systems which is representative for all the other metal decorations studied within this work. The reason to chose similar initial and final states as that for pristine was to investigate the role of the decorating atom on $E_{\text{ads-bar}}$ and ΔH_{ads} , *ceteris paribus*.

In the case of metal decorations, the $E_{\text{ads-bar}}$ is influenced by an additional factor other than the charge transfer between borophene and H_2 molecule, which is the steric effect of the decorating atoms. The steric effects contribute to non-bonding interactions between two reactants that can influence the reaction between them. Steric effects are directly proportional to the size of the decorating atom. Hence, larger atoms such as K have larger steric effect contributions than smaller atoms such as Li.

In the previous systems studied, the $E_{\text{ads-bar}}$ was only influenced by the charge on the B atoms that were close to the H_2 molecule. In metal decorations, however, it is seen that the B atoms close to the H_2 molecule are close to neutral in charge. Thus, the barrier height for chemisorption is determined by the steric factor, which is determined by the size of the decorating atom. In Table 4.4, q_0 is the charge on the B atoms before the addition of H_2 molecule while q_1 and q_2 are the charges on B and H atoms respectively in the chemisorbed state. As seen from the Table 4.4, the larger the atomic radius of the decorating metal, the higher is the barrier height. The minimum energy pathway for K decorated borophene is shown in Figure 4.8. The minimum energy pathway of the other metal atoms used for decoration are shown in Figures C.1, C.2, C.3 in Appendix C. The final chemisorbed state is stabilized by the inter-

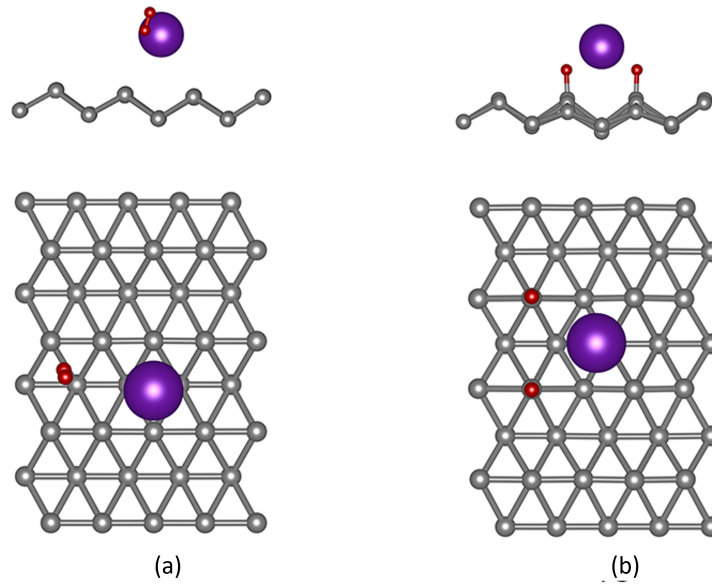


FIGURE 4.7: (a) Physisorbed and (b) chemisorbed states of H_2 on K decorated borophene. Grey spheres represent B atoms, red spheres, H atoms and K atoms are represented by purple spheres.

TABLE 4.4: Analysis on metal decorated systems.

Metal	q_0 [e]	$ q_1q_2 $ [e^2]	Atomic radius [\AA]	ΔH_{ads} [eV]	$E_{\text{ads-bar}}$ [eV]	$E_{\text{des-bar}}$ [eV]
Li	0.03	0.32	1.67	-1.22	0.62	1.84
Na	0.04	0.37	1.9	-1.19	0.64	1.83
K	0.03	0.37	2.43	-1.11	0.68	1.79
Ca	-0.03	0.4	1.94	-1.3	0.63	1.93

actions between the H atom and the B atom onto which the H is adsorbed. The absolute value of the product of the charges on the B and H atoms, which is proportional to the magnitude of the Coulombic interaction, are listed in the Table 4.4. It can be seen that with the increase in Coulombic interaction between B and H atoms, the stability of the chemisorbed state increases leading to the ΔH_{ads} values being more negative. The interaction between the metal atom and H atoms, however, makes the final state less stable. It can be posited that the above mentioned interaction is directly proportional to the size of the metal atom. This can be understood from the ΔH_{ads} value of Na and K which have similar $|q_1q_2|$ values. As K is a larger atom compared to Na, there is a higher interaction between K and the H atoms which leads to a lesser stable final structure and thus a lesser negative ΔH_{ads} .

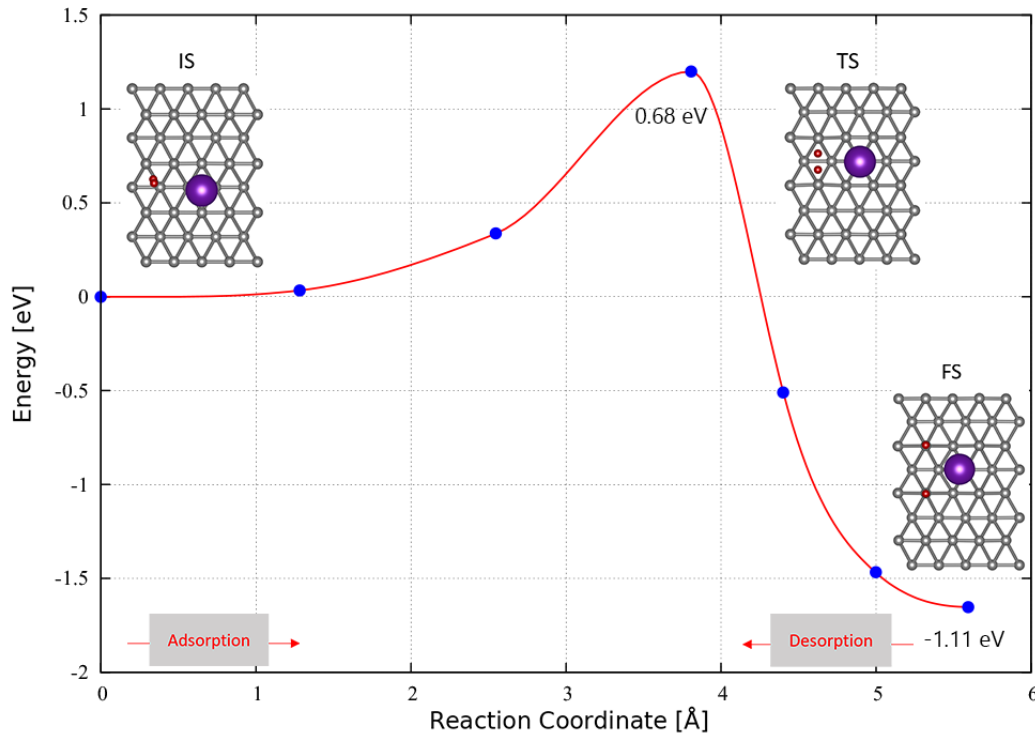


FIGURE 4.8: Minimum energy pathway corresponding to H_2 dissociation on K decorated borophene. For the reaction, the ΔH_{ads} and $E_{\text{ads-bar}}$ was found to be -1.11 eV and 0.68 eV respectively.

4.4 Double metal decorations

From the study of Qin *et al.* [29], it was seen that adding charges reduces the $E_{\text{ads-bar}}$. However, it was also shown that there would be an decrease in ΔH_{ads} . As the aim of this study is to reduce both $E_{\text{ads-bar}}$ and $|\Delta H_{\text{ads}}|$, decoration of two metal atoms was studied with the metal atoms arranged so as to increase the interactions of metal atoms with the chemisorbed H atoms to make the final state less stable. Adsorption energy of a second metal atom on a single decorated substrate ($E_{\text{ads}}^{2\text{M}}$) is

$$E_{\text{ads}}^{2\text{M}} = E_{\text{substrate}+2\text{M}} - E_{\text{substrate}+\text{M}} - E_{\text{M}} \quad (4.5)$$

where $E_{\text{substrate}+2\text{M}}$ is the total energy of substrate with two metal atoms and the other symbols have the same meaning from the previous equations. $E_{\text{ads}}^{2\text{M}}$ values for the metal atoms used in this work is listed in Table 4.5. From Table 4.5 it can be understood that the addition of a second decorating metal on the single decorated borophene system is energetically favourable.

The configurations for K double decorated system are shown in the Figure 4.9. As mentioned before, the configurations in Figure 4.9 is representative for all the other double metal decorations systems studied within this work. The minimum energy pathway for K decorated borophene is shown in Figure 4.10. The minimum energy pathway of the other metal atoms used for

TABLE 4.5: Adsorption energies of second metal atom on single decorated borophene systems.

Metal	$E_{\text{ads}}^{2\text{M}}$ [eV]
Li	-1.38
Na	-1.31
K	-1.59
Ca	-1.33

decoration are shown in Figures C.4, C.5, C.6 in Appendix C. The $E_{\text{ads-bar}}$ val-

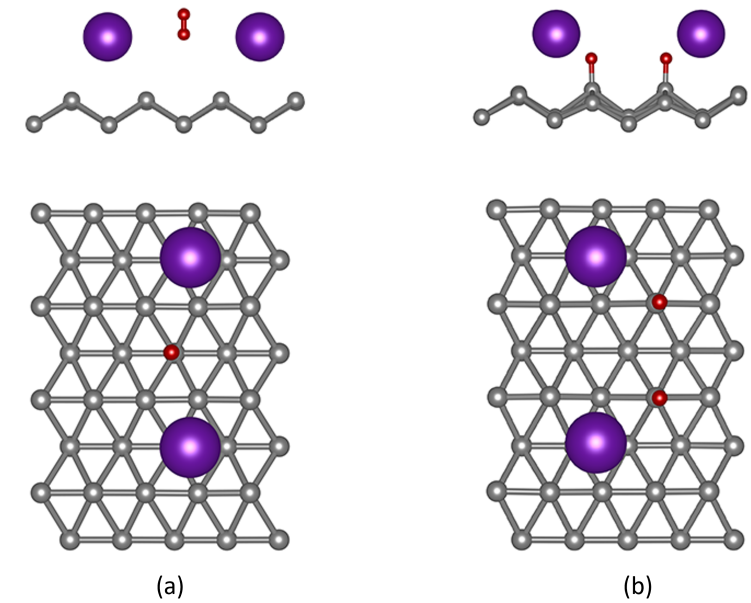
FIGURE 4.9: (a) Physisorbed and (b) chemisorbed states of H_2 on double K decorated borophene.

TABLE 4.6: Analysis on double metal decorated systems.

Metal	q_0 [e]	$ q_1 q_2 $ [e^2]	Atomic radius [\AA]	ΔH_{ads} [eV]	$E_{\text{ads-bar}}$ [eV]	$E_{\text{des-bar}}$ [eV]
Li	0.21	0.38	1.67	-1.19	0.76	1.95
Na	0.2	0.39	1.9	-1.09	0.73	1.82
K	0.17	0.4	2.43	-1.00	0.73	1.73
Ca	0.36	0.38	1.94	-1.00	0.8	1.8

ues for double metal decorated systems are obtained to be higher than that for single decorated ones. The additional steric factor due to the presence of two metal atoms may be a reason for this. As discussed previously, the final chemisorbed state is affected by the interaction between the decorating

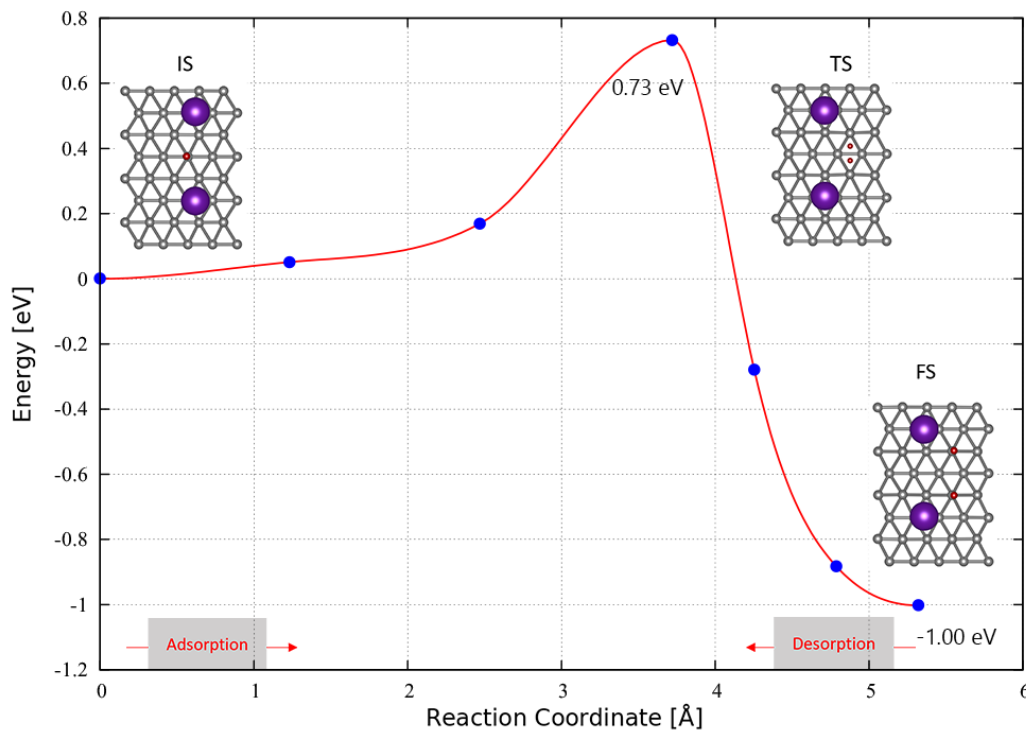


FIGURE 4.10: Minimum energy pathway corresponding to H₂ dissociation on double K decorated borophene. For the reaction, the ΔH_{ads} and $E_{\text{ads-bar}}$ was found to be -1.00 eV and 0.73 eV respectively.

atoms and H atoms as well as the Coulombic interaction between the H and the B atoms. From Table 4.6, it is seen that the $|q_1q_2|$ values of the four metal decorated configurations are similar. The differences in the ΔH_{ads} of the dissociated state is thus mainly influenced by the interactions between the metal and H atoms, with the larger atoms leading to a lesser negative ΔH_{ads} compared to the smaller decorating atoms which increases the reversibility of the chemisorption reaction. Double K decorated system reduced $|\Delta H_{\text{ads}}|$, $E_{\text{ads-bar}}$ and $E_{\text{des-bar}}$ values by 28%, 4% and 20% respectively when compared with the pristine borophene system.

4.5 Discussion

4.5.1 Range of energies

As mentioned before, several configurations were tested to find the most stable initial and final states. Range of a set of values is calculated as the difference between the highest and lowest values. The range of the energies for the initial and final states for the pristine, single and double vacancy configurations are listed in the Table 4.7. It can be seen that the range of energies for physisorbed states is lower than that for the chemisorbed state. This shows

TABLE 4.7: Range of energies for pristine, SV and DV configurations in eV.

Systems	Physisorption [eV]	Chemisorption [eV]
Pristine	0.003	1.9
SV	0.01	1.0
DV	0.03	1.23

that when the H_2 molecule is physisorbed, it is less sensitive to the adsorption site as compared to the chemisorbed state.

4.5.2 Charge transfer

The charge present on the H atoms in the physisorbed and the chemisorbed states were studied and the results are plotted in the Figure 4.11. From the

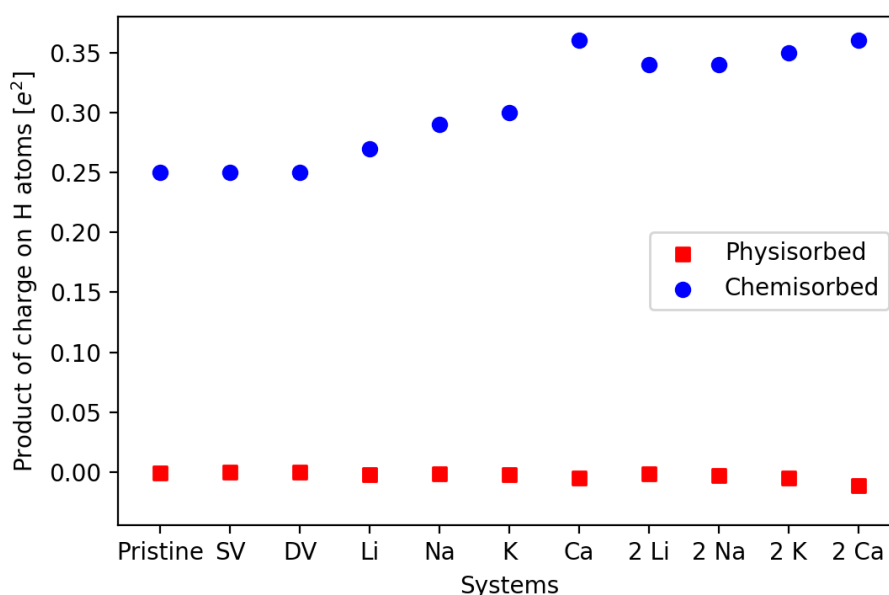


FIGURE 4.11: Product of charge on H atoms for the various systems studied.

above figure, it can be seen that the product of the charges on the two H atoms in the physisorbed state is close to zero for all the cases studied in this work. The negative sign of the product shows that the two H atoms are oppositely charged.

Analysing the charges on the H atoms in the chemisorbed state, it can be seen that with the addition of charge onto the system by the decorating atom, there is an increase in the magnitude of the product of the charges present on the two chemisorbed H atoms. The positive sign of the product indicates that both the H atoms are similar in charge and from the charge analysis one can confirm that they both are negatively charged due to the transfer of electrons from the borophene substrate to the H atoms.

4.5.3 Adsorption energies

The adsorption energies of H_2 molecules on various borophene systems are calculated by Equation. 4.1 and are plotted in the Figure 4.12. It can be seen

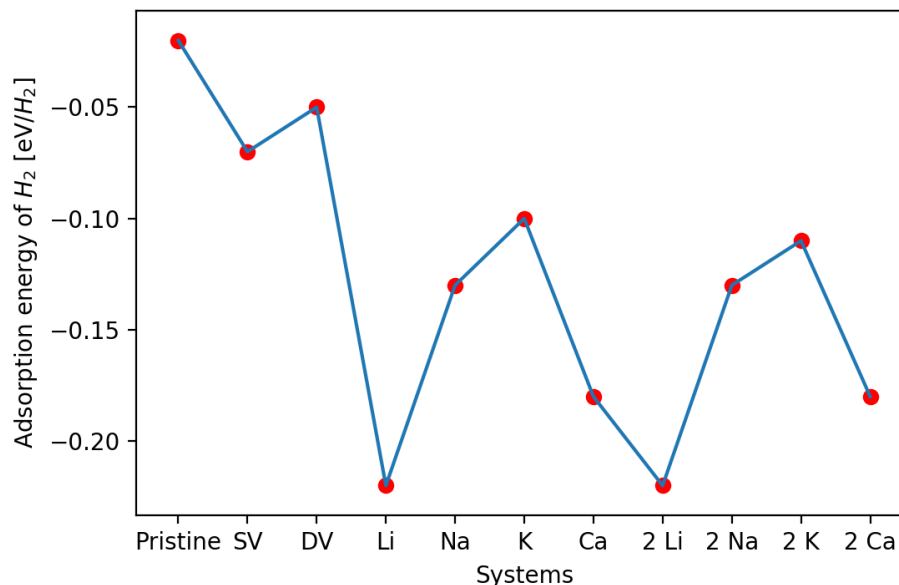


FIGURE 4.12: Adsorption energies of H_2 on various systems studied.

from the figure that metal decorations increases the magnitude of the adsorption energy as there is increased polarization induced by the charge transferred from the metal atoms, leading to an increased interaction between the H_2 molecule and the substrate. Li has the maximum magnitude of adsorption energy as seen from Figure 4.12. It is also worth noting that single metal decoration and double metal decoration have similar H_2 adsorption energies. This is because the magnitude of H atom polarization is similar for single and double metal decorated systems studied within this work as seen in Figure 4.11.

4.5.4 Distances and bond lengths

D_{H-H} values

The distances between the H atoms in the physisorbed and the chemisorbed states are plotted in the Figure 4.13. On comparing the D_{H-H} values in the physisorbed and chemisorbed state, it can be seen that distances between H atoms in the physisorbed state for the configurations studied have a low range of 0.02 Å. On the other hand, the range for D_{H-H} values in the chemisorbed state is 0.38 Å. This is an indication of the stronger interactions between H atoms in the physisorbed state than in the chemisorbed state. The reason for this might be because, in the chemisorbed state, the H atoms interact strongly with the adsorbed B atoms leaving little scope for the two H atoms to interact.

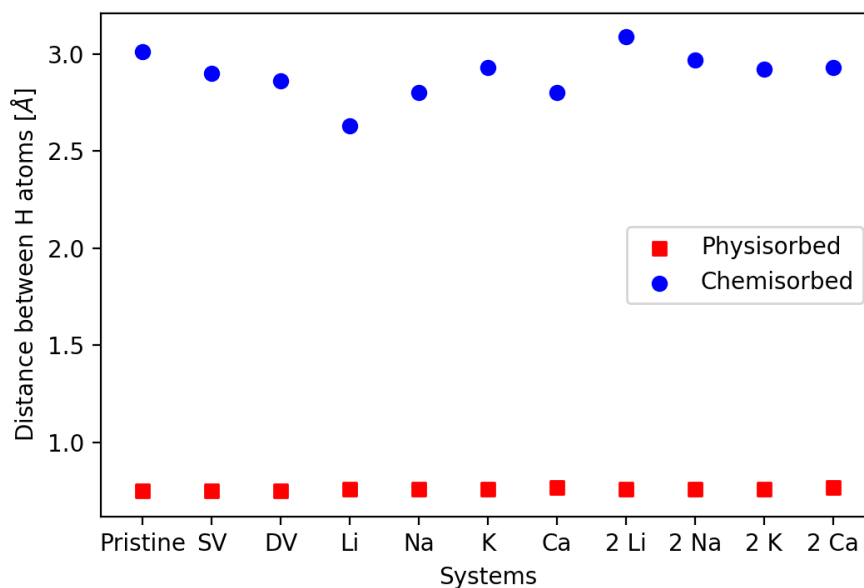


FIGURE 4.13: Distance between H atoms for the various systems studied.

D_{B-H} values

The distances between the B atoms in the borophene substrate and the H atoms in the physisorbed and the chemisorbed states are plotted in the Figure 4.14. Since the B atoms and H atoms in the physisorbed state interact via

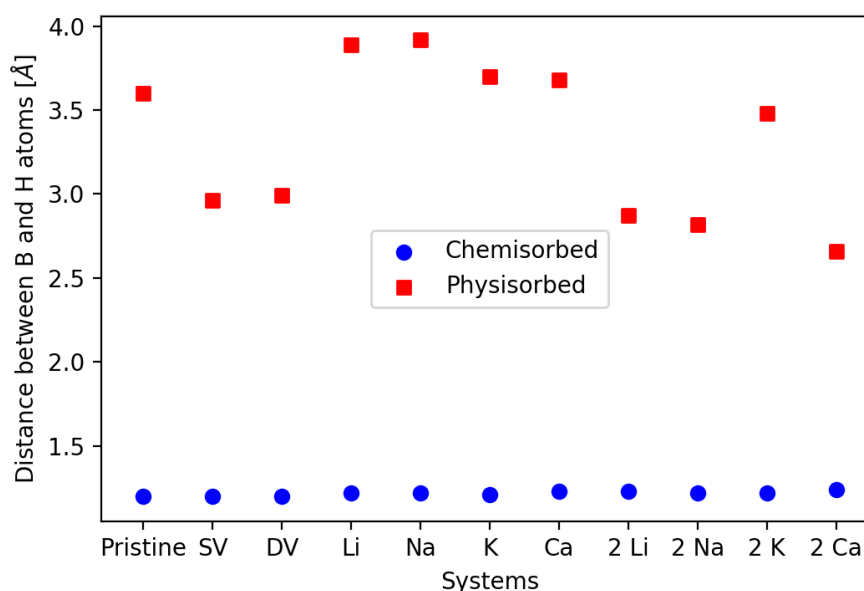


FIGURE 4.14: Distance between borophene and the H atoms for the various systems studied.

van der Waals forces, the distance between them across all the configurations studied has a large range of 0.94 Å. The D_{B-H} values for the chemisorbed state for the configurations examined has a range of only 0.04 Å which strengthens

the earlier conclusion of strong interaction between B and H atoms in the chemisorbed state.

4.5.5 Density of states

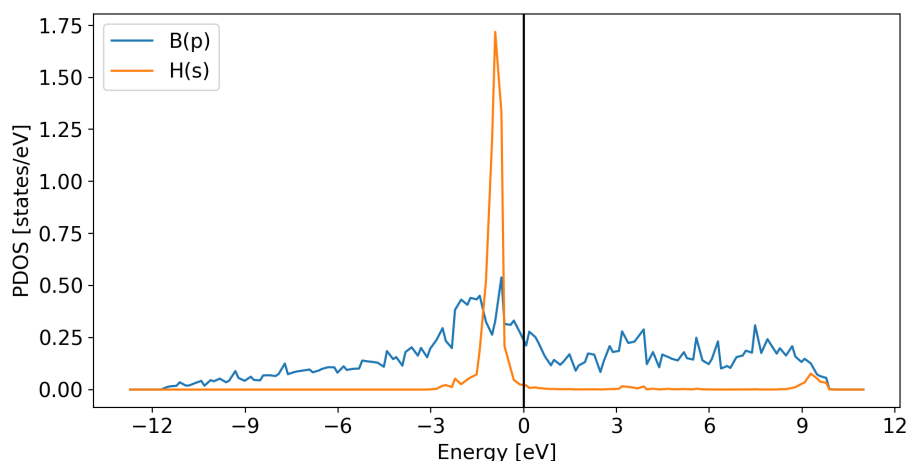


FIGURE 4.15: PDOS of B(p) and H(s) in H_2 physisorbed pristine borophene system with the black vertical line being the Fermi level.

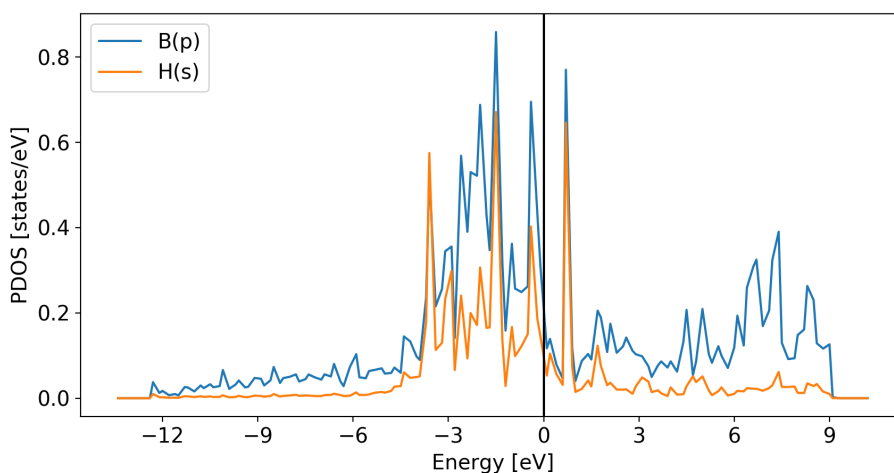


FIGURE 4.16: PDOS of B(p) and H(s) in H_2 chemisorbed pristine borophene system with the black vertical line being the Fermi level.

The partial density of states (PDOS) of the p-orbital of the boron atoms directly interacting with the H atoms and the PDOS of s-orbitals of H atoms are shown above. Figure 4.15 represents the physisorbed state and Figure 4.16 represents the chemisorbed state. On comparing both the PDOS for the pristine borophene, it can be seen that there is a broadening and overlapping of the H(s) peaks with the B(p) peaks in the chemisorbed state which indicates hybridisation and covalent bonding between the H and B atoms. Also,

a shifting of the H(s) peaks closer to the Fermi level in the chemisorbed state, indicates a weakening of the H-H bond.

4.5.6 ΔH_{ads} , $E_{\text{ads-bar}}$ and $E_{\text{des-bar}}$ values

The ΔH_{ads} , $E_{\text{ads-bar}}$ and $E_{\text{des-bar}}$ of the various systems studied are plotted in the Figure 4.17. The negative values of the ΔH_{ads} indicate that the final states

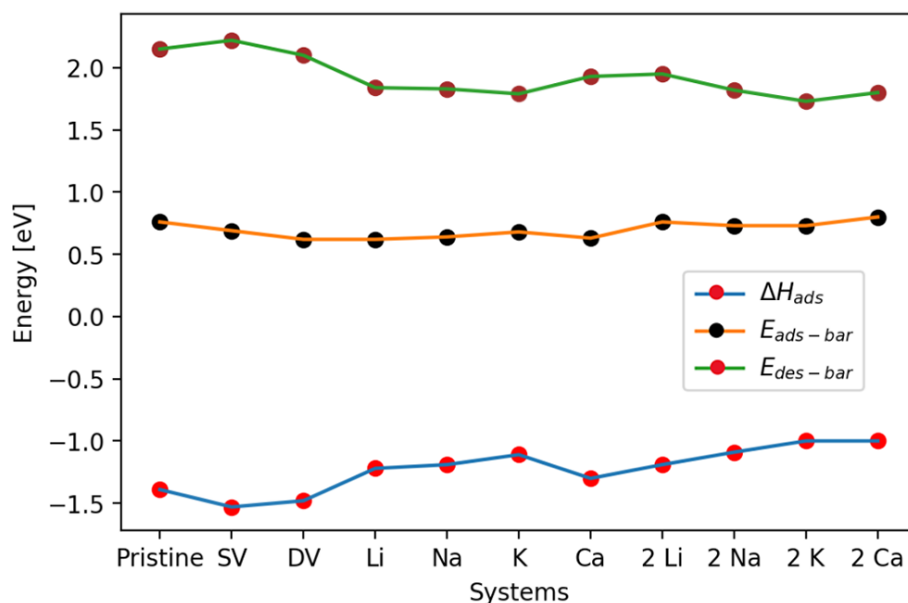


FIGURE 4.17: ΔH_{ads} , $E_{\text{ads-bar}}$ and $E_{\text{des-bar}}$ values of the systems studied.

are more energetically stable than the initial states. As seen from the earlier sections, metal decorations makes the ΔH_{ads} values less negative (increases the reversibility of the reaction) due to the interactions between the metal and H atoms. This trend can be noted from the figure, where the bigger atoms tend to have lesser negative ΔH_{ads} values compared to the smaller atoms. An exception in this trend is single decorated Ca which due to its large charge transfer to the borophene substrate, stabilizes the final chemisorbed state thus making the ΔH_{ads} more negative.

The $E_{\text{ads-bar}}$ values are also plotted in Figure 4.17. As discussed earlier, double metal decorated systems exhibit a higher $E_{\text{ads-bar}}$ value (decreases the reversibility) compared to the single metal decorated systems. From the $E_{\text{des-bar}}$ curve, it can be understood that single and double K decorated system performs the best in terms of desorption barrier height reducing the $E_{\text{des-bar}}$ value by 17% and 20% respectively with respect to the pristine borophene system.

4.5.7 Possible applications

As discussed earlier, hydrogen has a negative Joule-Thomson coefficient. This leads to the heating up of hydrogen gas as it moves from a region of high

pressure to that of low pressure. Due to this phenomenon, filling hydrogen into a tanker on a transporting truck leads to the heating up of the tank. Li *et al.* [8], used theoretical and experimental methods to quantitatively analyse the final temperatures. It was shown that temperatures close to 450 K can be reached during the adiabatic expansion of the hydrogen gas. Sheets of borophene fitted in the compression container is an option to effectively use up this heat. Borophene can use the temperature rise in the container to chemisorb hydrogen atoms onto itself, aiding the hydrogen storage process. Investigations of the stability of borophene at increased temperature and pressure and the behaviour of chemisorption with various flow rates must be done to analyse the feasibility of the above idea. Also, how metal decorations on the borophene systems behave under high temperatures is a study that can be done.

Metal hydrides which are considered as an option for long term hydrogen storage have an exothermic hydrogen adsorption process. A system with metal hydrides with borophene sheets may also be a viable option for hydrogen storage.

Chapter 5

Conclusion

Systems that were studied in this thesis work were classified into four categories: pristine, defective, metal decorated and double metal decorated borophene. The main objective of the study was to increase the reversibility of the chemisorption reaction by reducing the $E_{\text{ads-bar}}$ value and bringing the $|\Delta H_{\text{ads}}|$ value close to zero. The conclusions of the study on the four categories based on their ΔH_{ads} , $E_{\text{ads-bar}}$ and $E_{\text{des-bar}}$ are mentioned in this section.

For the hydrogen adsorption on pristine borophene, the low adsorption energy (-0.02 eV/ H_2) of H_2 on borophene indicates a weak interaction between the physisorbed H_2 molecule and the substrate. The ΔH_{ads} was found to be -1.39 eV while the $E_{\text{ads-bar}}$ is 0.76 eV leading to a $E_{\text{des-bar}}$ of 2.15 eV.

Vacancy creation in the borophene system was investigated with a single vacancy and double vacancy systems. Both the systems showed a lowering of the $E_{\text{ads-bar}}$ and an increase in the magnitude of ΔH_{ads} due to the increased charge present on the B atoms interacting with the H_2 molecule, compared with the pristine case. The SV and the DV systems exhibited $E_{\text{des-bar}}$ of 2.22 eV and 2.1 eV respectively.

Metal decoration on pristine borophene leads to a less negative ΔH_{ads} values compared to pristine and vacancy systems. This is due to the influence of the charge transfer from the metal atom to the substrate as well as the interaction between the metal and H atoms. The $E_{\text{ads-bar}}$ is influenced by the steric effects of the metal atom. Among the metal atoms studied, K leads to the smallest $E_{\text{des-bar}}$ value (1.79 eV), which is a 17% improvement compared to the corresponding value for the pristine system.

Double metal decoration on the borophene systems showed an increase in the $E_{\text{ads-bar}}$ compared to the single metal decorated case. This may be due to the additional steric effects of having two metal atoms on the system. The final chemisorbed states were less stable than that for a single decorated case which could be understood from the less negative ΔH_{ads} values. Among the double metal decorated systems, K atom showed the least $E_{\text{des-bar}}$ value (1.73 eV), which is a 20% improvement with respect to the corresponding value for the pristine system.

The physisorption and chemisorption of H_2 on various borophene systems were also studied with the help of Bader charge analysis, bond length calculations and partial density of states. From the analysis it was understood that H atoms are adsorbed on top of the borophene sheet via weak van

der Waals forces in the physisorbed state and in the chemisorbed state, the H atoms are strongly bonded to the B atoms of the substrate via covalent bonds.

Chapter 6

Recommendations

In this section, the recommendations for future studies are listed.

1. In this work, metal decorations were used to reduce the $E_{\text{des-bar}}$ on pristine borophene. Double K decoration was able to reduce this barrier height to 1.73 eV which is 20% lesser than the corresponding value for pristine borophene. However, there was a trade off between the ΔH_{ads} and $E_{\text{ads-bar}}$ within metal decorated borophene systems as the reduction in the magnitude of ΔH_{ads} (increase in the reversibility of the reaction) brought about an increase in $E_{\text{ads-bar}}$ (decrease in the reversibility). This was one of the reasons why the $E_{\text{des-bar}}$ could not be reduced further. More options could be investigated to reduce the $E_{\text{des-bar}}$, one of which could be the use of different metal decorations on the same borophene sheet to fine-tune the interactions between the H and metal atoms.
2. Using partially hydrogenated borophene for hydrogen chemisorption is another option that can be examined for hydrogen chemisorption. The additional charge present on the B atoms may be distributed among the H atoms bonded to the borophene substrate, thus minimizing the interaction between the incoming H atoms and reducing the $|\Delta H_{\text{ads}}|$ of the chemisorption reaction.
3. As seen in the methodology section, a 6×3 supercell performs better than a 4×5 supercell in terms of system size effects. The former also has a lesser number of atoms than the latter. This leads to a reduction in the computational load of the simulations.
4. As seen in the earlier discussions, the B atoms around vacancies are more negatively charged which aids in the chemisorption reaction by reducing the $E_{\text{ads-bar}}$ value compared to the pristine systems. However, the ΔH_{ads} values are more negative in this case as with more charge transfer from the B atoms to the H atoms, the final chemisorbed state becomes more stable, reducing the reversibility of the reaction. Metal decorations was seen to increase the steric hindrances for the chemisorption reaction, thus increasing the $E_{\text{ads-bar}}$ value. It also made the final chemisorbed state less stable, decreasing the $|\Delta H_{\text{ads}}|$ value. Metal decorations on single and double vacancy systems can thus be an interesting study to analyse.

5. The striped borophene structure was examined for this study. Other structures such as the β_{12} and χ_3 which have a lower density of boron atoms compared to striped borophene can also be examined for hydrogen chemisorption.
6. Ab initio molecular dynamics (AIMD) studies can further the understanding of the systems and throw light on their temperature-dependent properties.
7. As mentioned earlier, some of the established technologies generate heat during the adsorption process. The scope of incorporating metal decorated borophene sheets within the same system can be examined. Also, how hydrogen chemisorption on borophene sheets is influenced by varying pressure, temperature and flow rates can be investigated.

Appendix A

Configurations

A.1 Pristine

The configurations examined for pristine physisorption are listed in Figure A.1. The configurations examined for pristine chemisorption are listed in

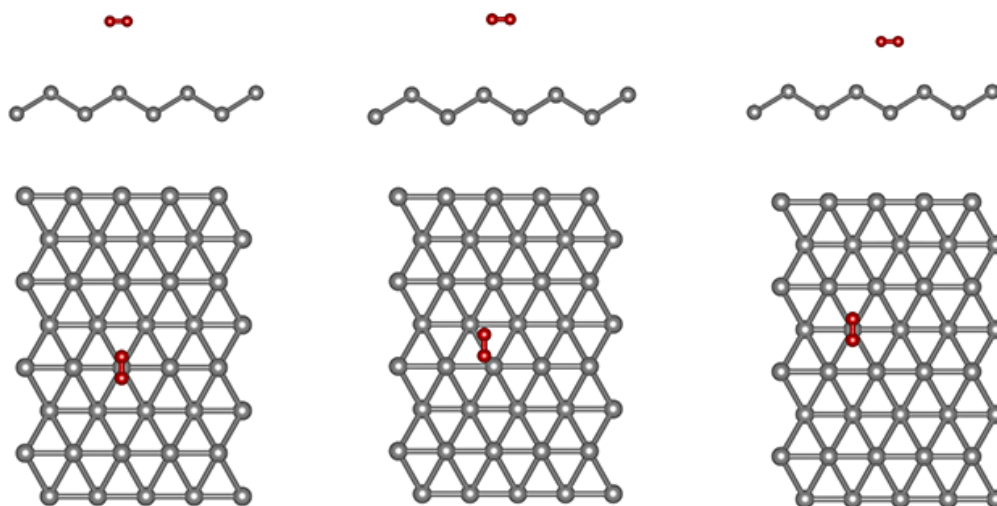


FIGURE A.1: Configurations for pristine physisorption.

Figure A.2.

A.2 Single vacancy

The configurations examined for single vacancy physisorption are listed in Figure A.3.

The configurations examined for single vacancy chemisorption are listed in Figure A.3.

A.3 Double vacancy

The configurations examined for double vacancy physisorption are listed in Figure A.5.

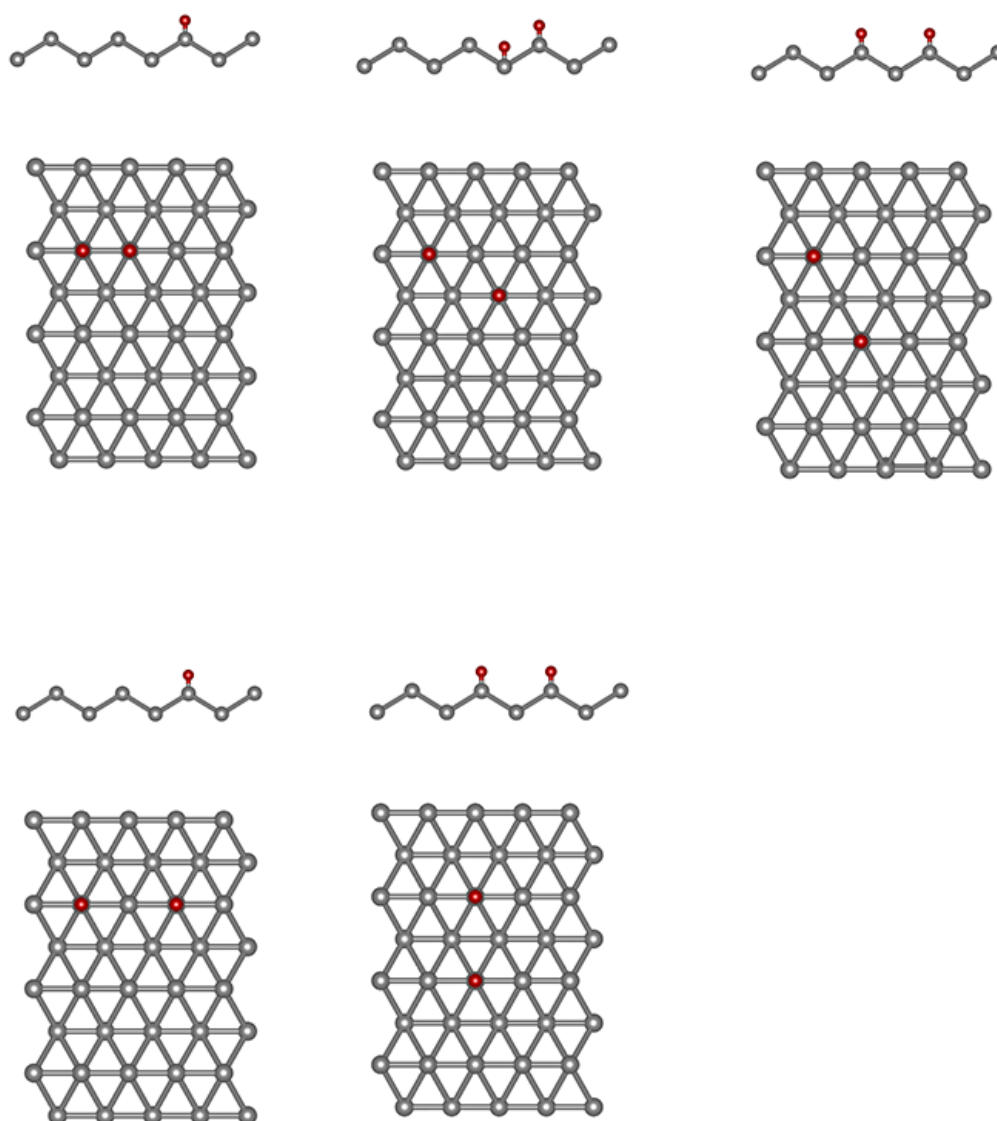


FIGURE A.2: Configurations for pristine chemisorption.

The configurations examined for double vacancy chemisorption are listed in Figure A.6.

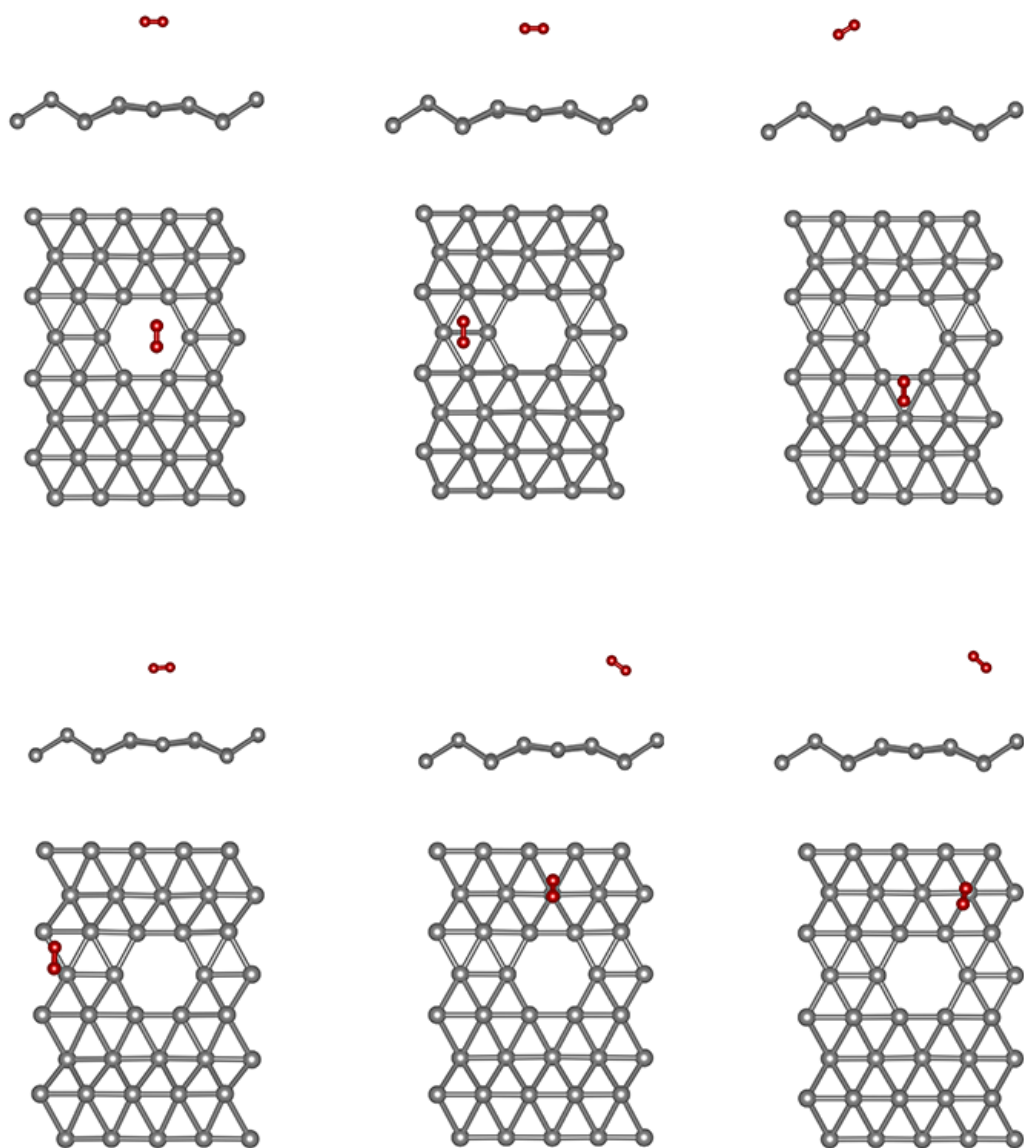


FIGURE A.3: Configurations for SV physisorption.

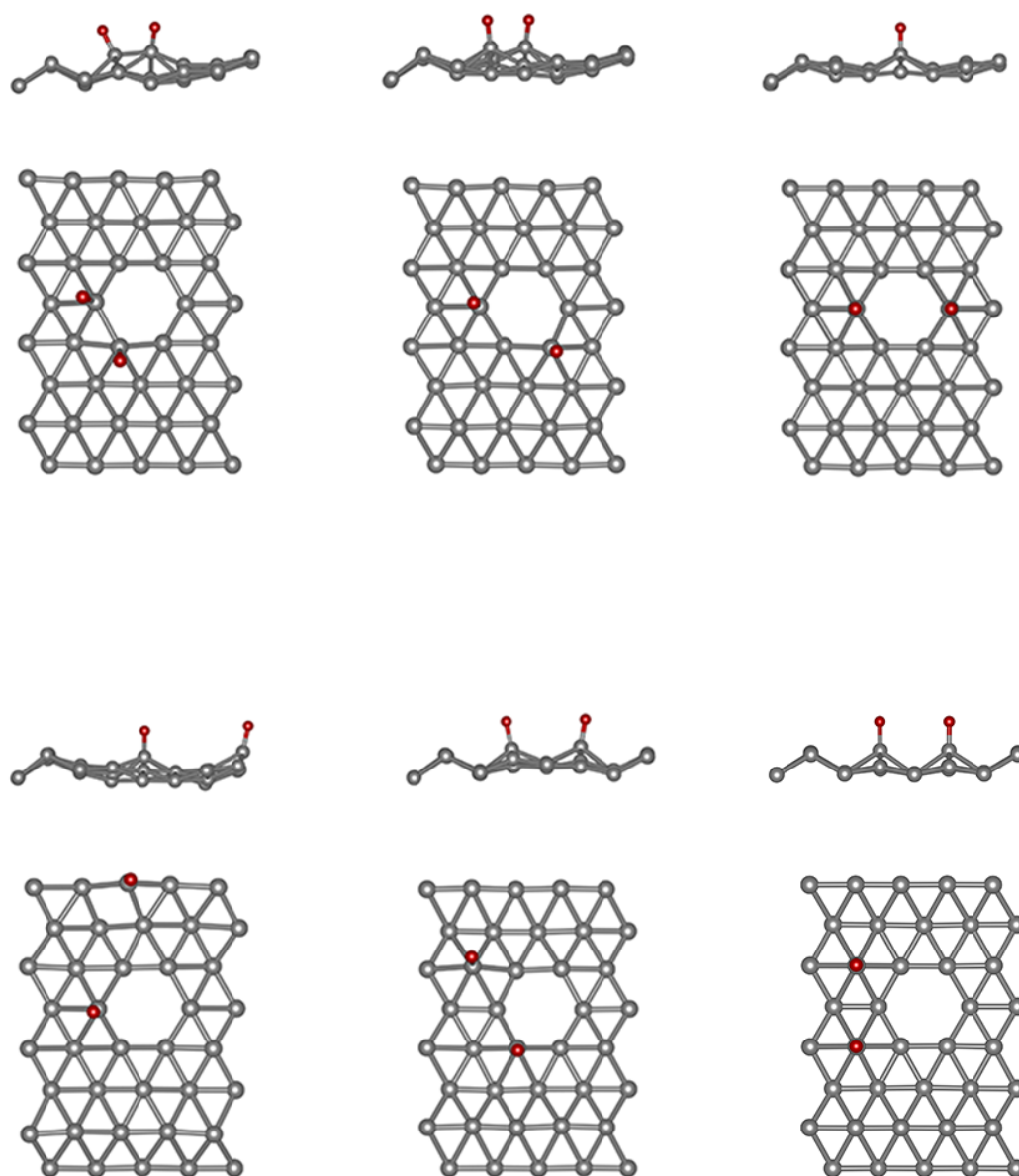


FIGURE A.4: Configurations for SV chemisorption.

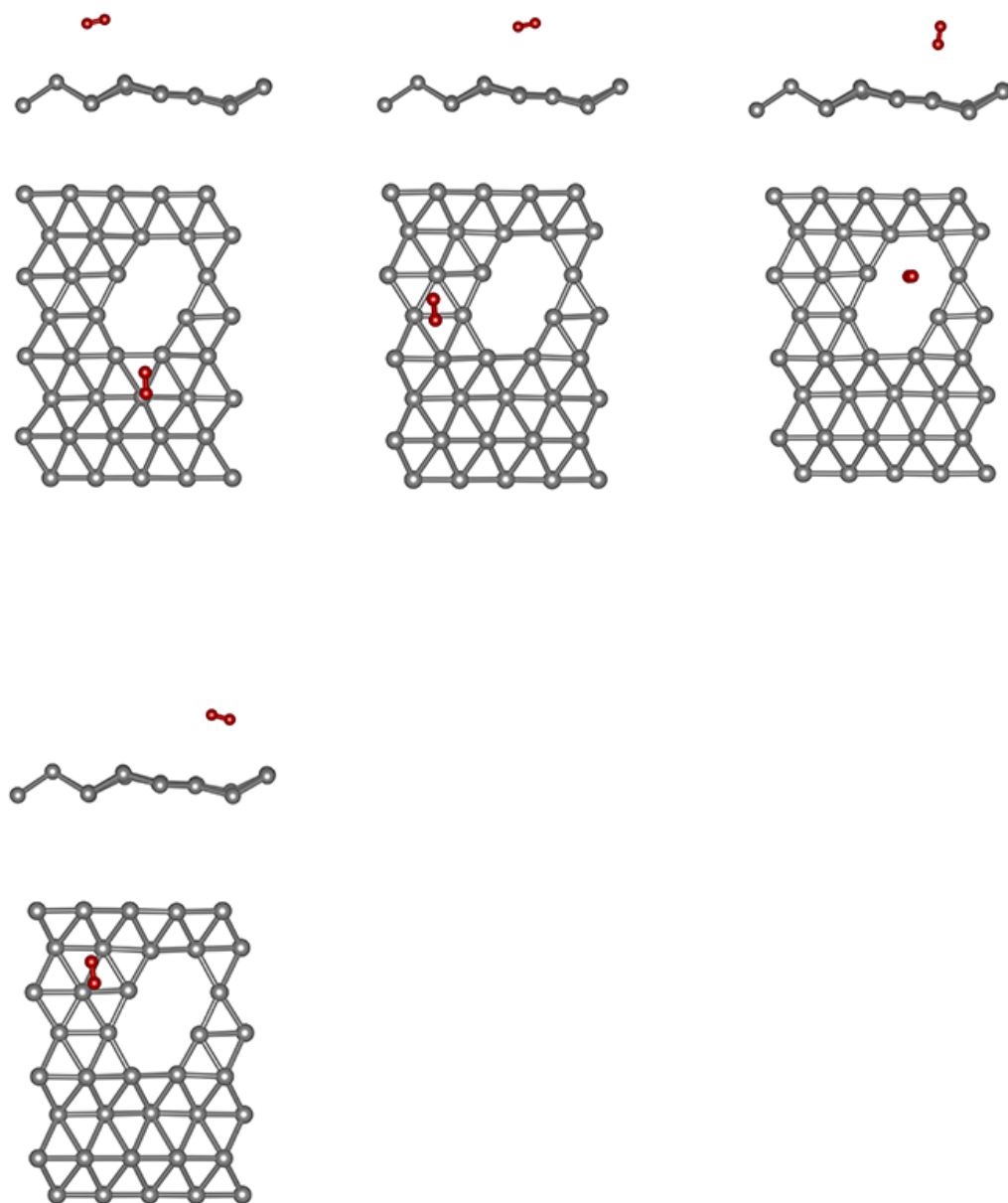


FIGURE A.5: Configurations for DV physisorption.

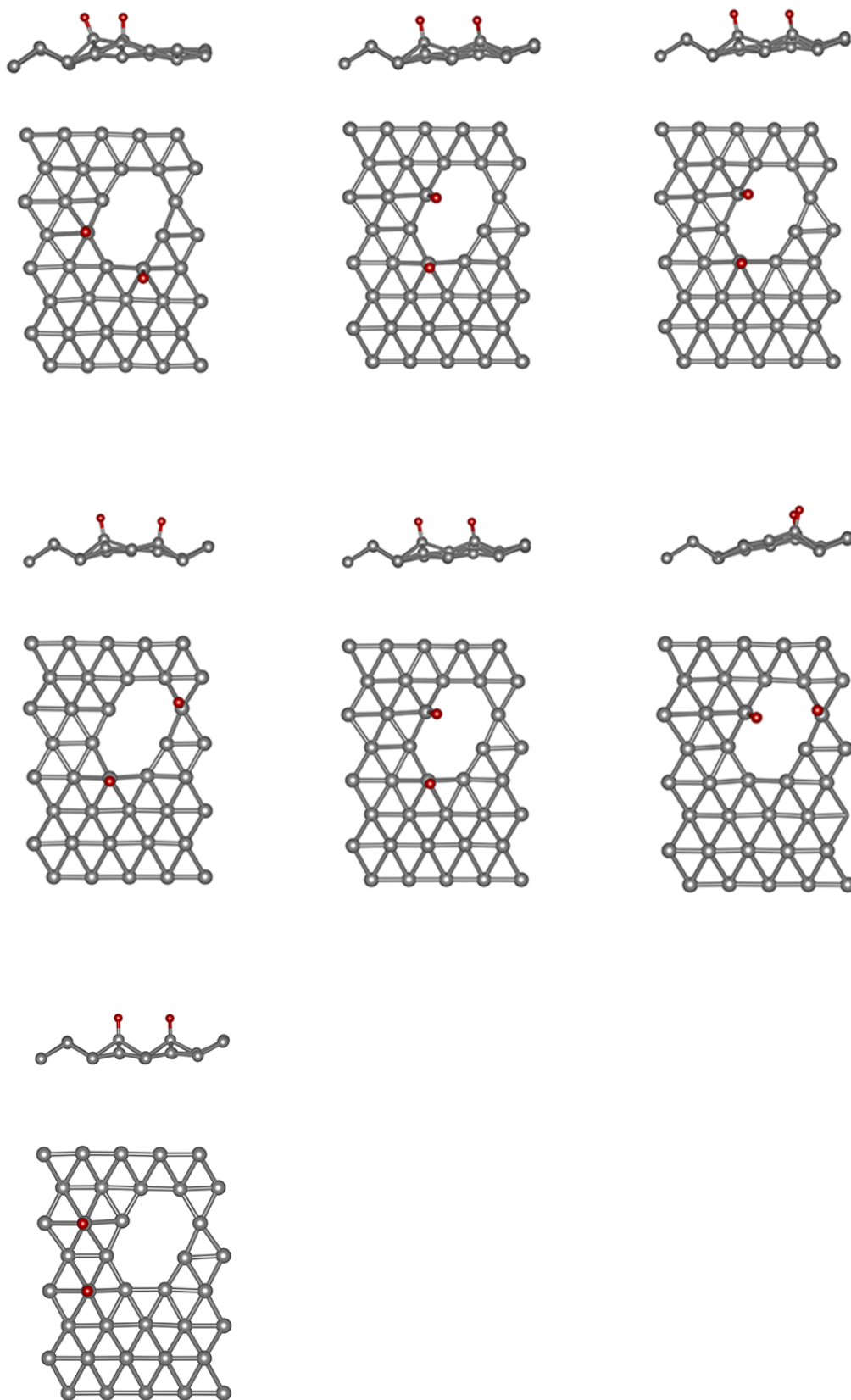


FIGURE A.6: Configurations for DV chemisorption.

Appendix B

Bash scripts

This section includes bash scripts that were used during the post-processing of the results.

```
#!/bin/bash
#author-THG Saji

for num in ./*;

do
cd ${num}
i="${num##*/}"
if grep -q accuracy OUTCAR; then
E=$(tail -n1 OSZICAR | awk '{print $5}')
echo "$i","$E" >> ../energies.csv
else
echo "$i", "Not converged" >> ../energies.csv
fi
cd ..
done
```

FIGURE B.1: Script to obtains energies from folders within.

```
#!/bin/bash
#author-THG Saji

for num in ./*;

do
cd ${num}
i="${num##*/}"
if grep -q accuracy OUTCAR; then
E=$(tail -n1 OSZICAR | awk '{print $5}')
echo "$i","$E" >> ../energies.csv
else
echo "$i", "Not converged" >> ../energies.csv
fi
cd ..
done
```

FIGURE B.2: Script to obtains time taken for calculations from folders within.

Appendix C

NEB of metal decorations

This section includes NEB images of metal decorations not included in the main text.

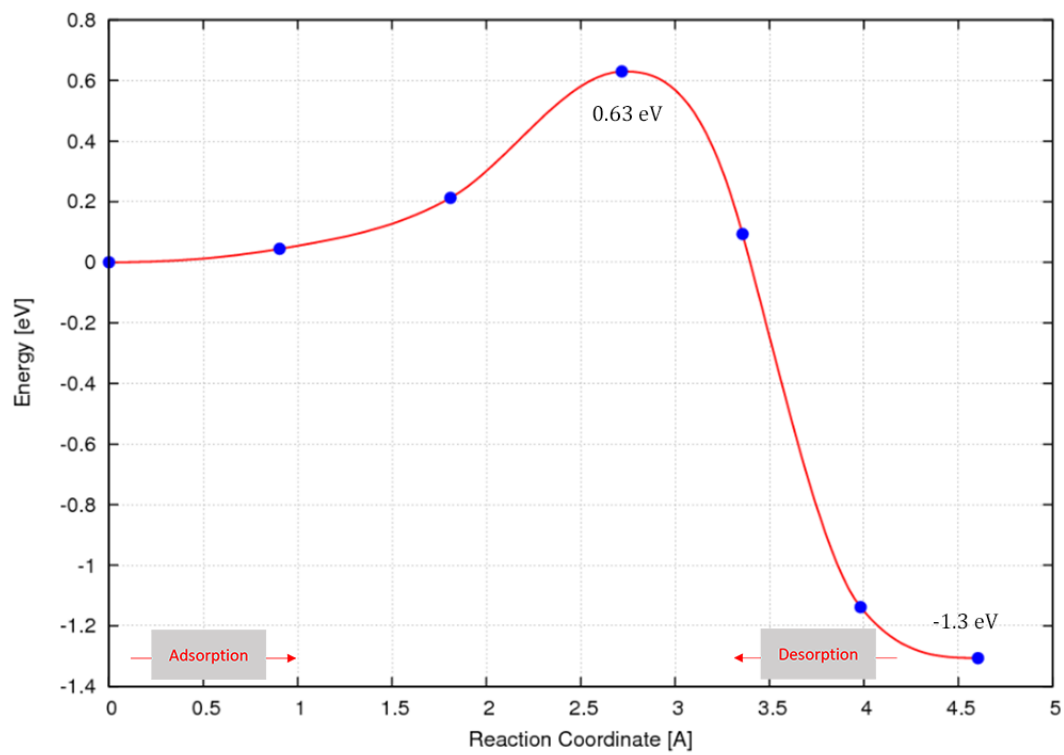


FIGURE C.1: Minimum energy pathway corresponding to H_2 dissociation on Ca decorated borophene.

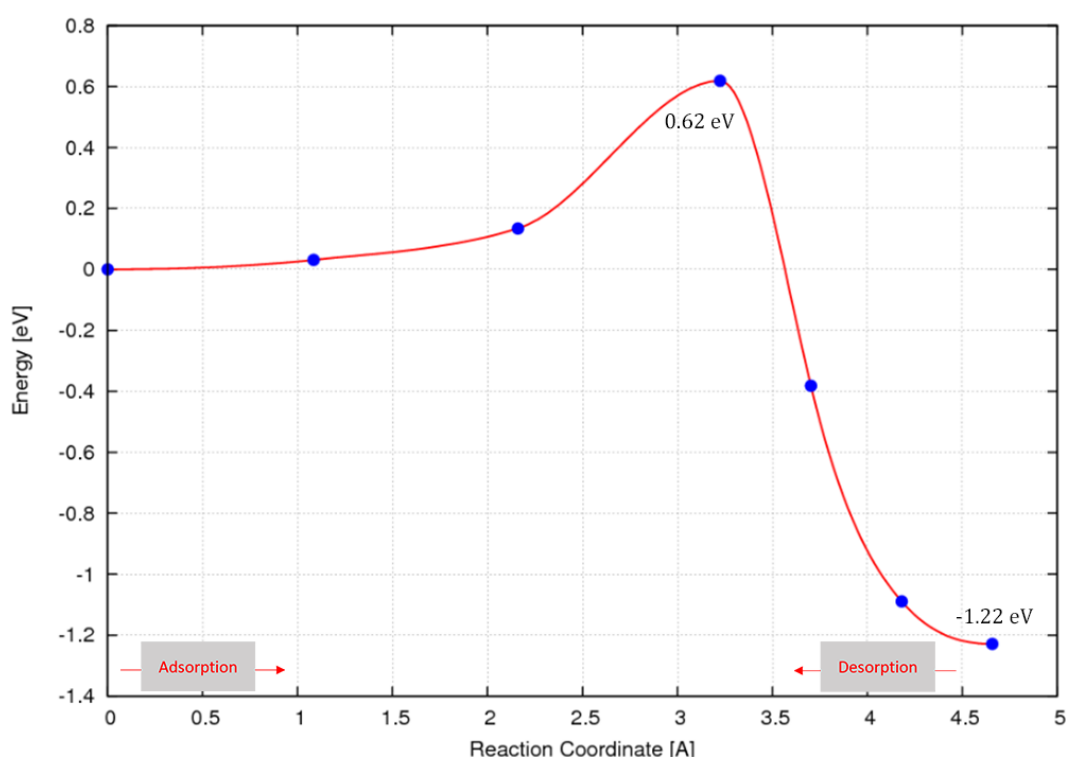


FIGURE C.2: Minimum energy pathway corresponding to H_2 dissociation on Li decorated borophene.

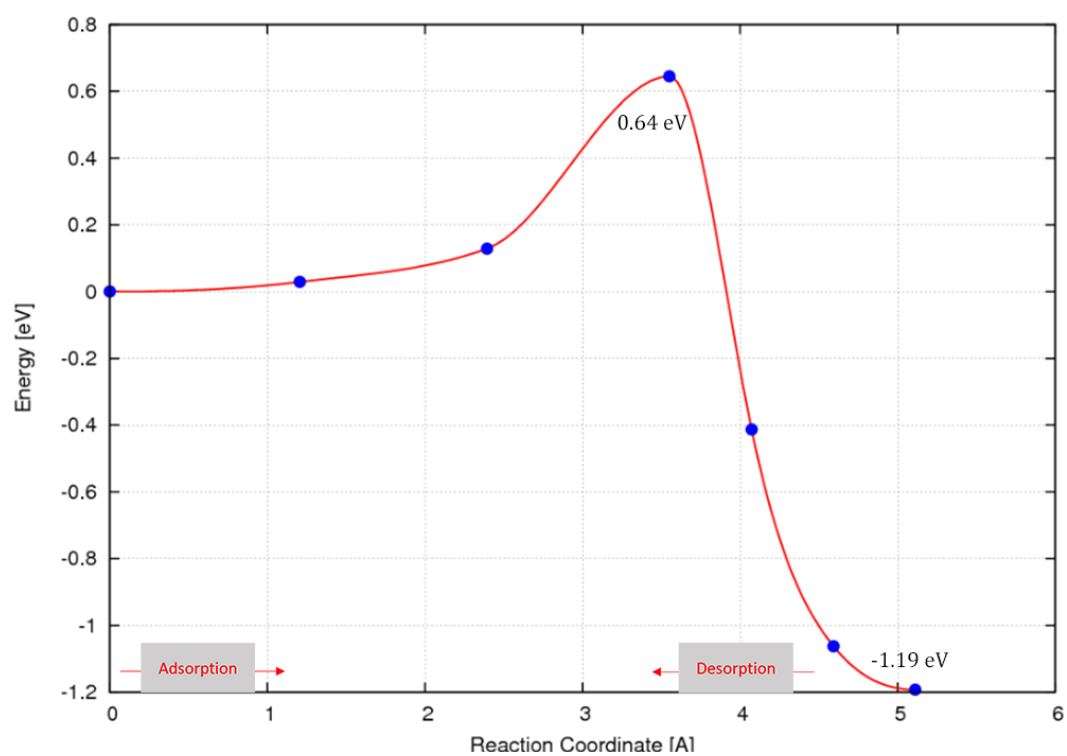


FIGURE C.3: Minimum energy pathway corresponding to H_2 dissociation on Na decorated borophene.

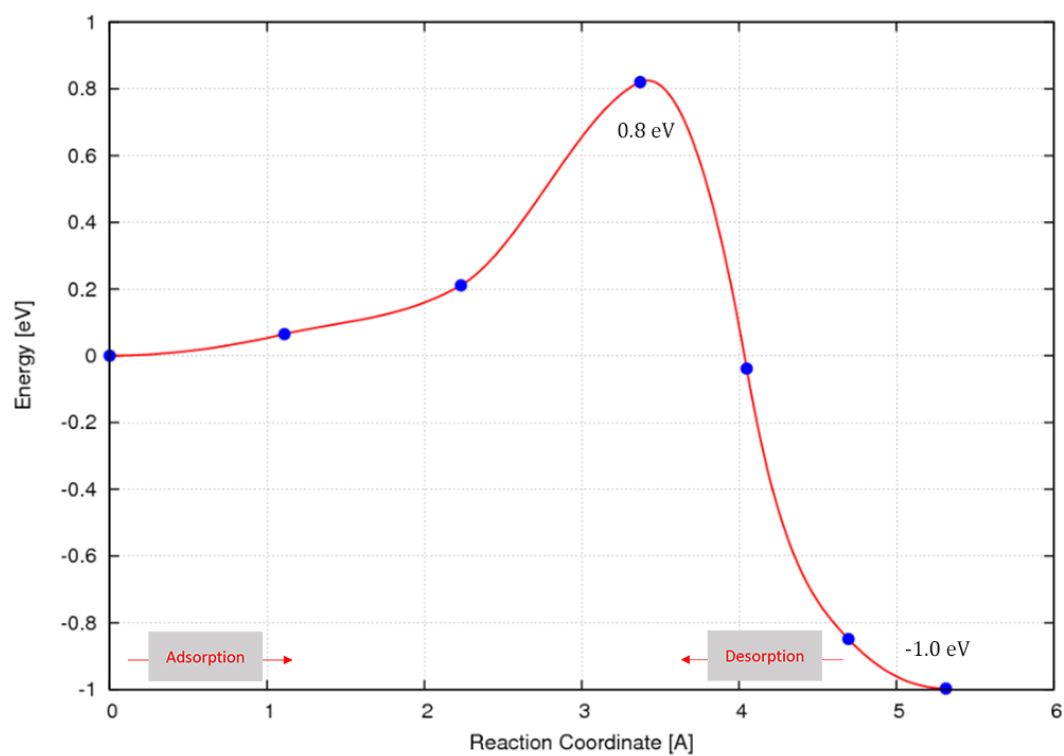


FIGURE C.4: Minimum energy pathway corresponding to H₂ dissociation on double Ca decorated borophene.

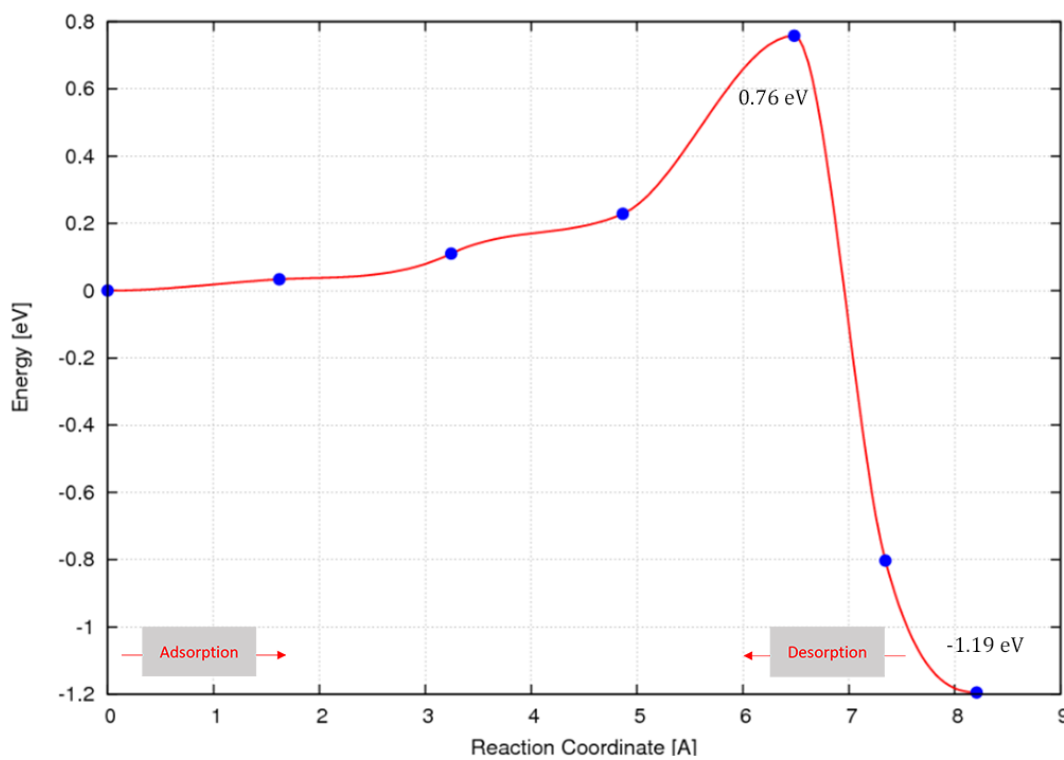


FIGURE C.5: Minimum energy pathway corresponding to H₂ dissociation on double Li decorated borophene.

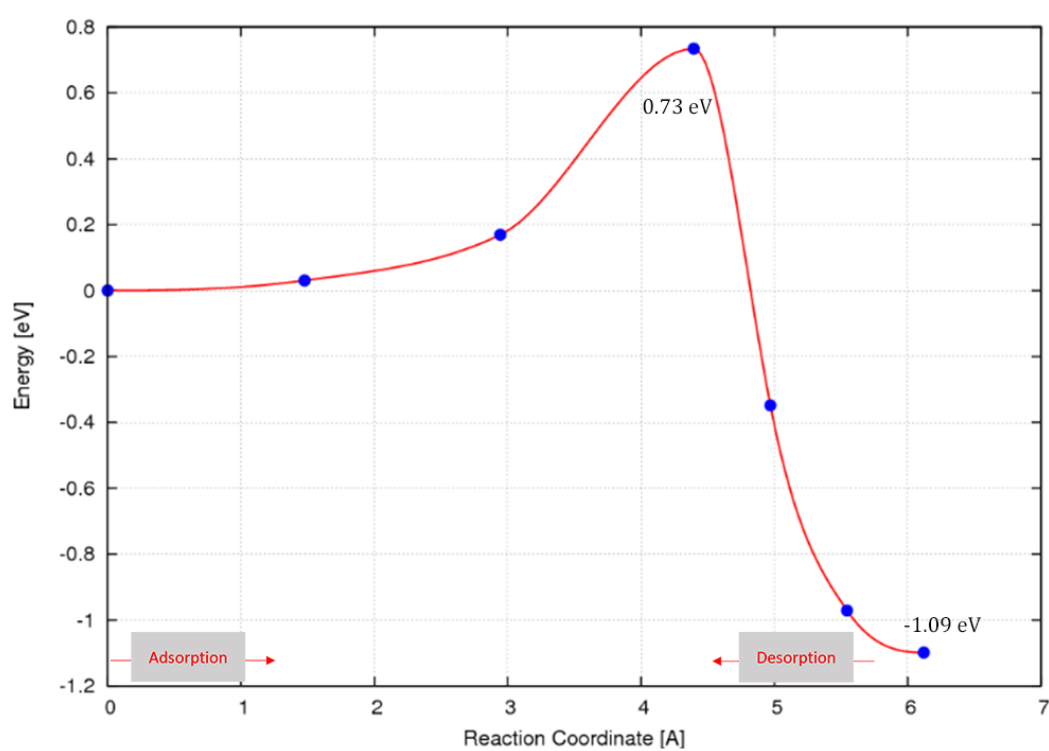


FIGURE C.6: Minimum energy pathway corresponding to H_2 dissociation on double Na decorated borophene.

Appendix D

Sensitivity analysis

The sensitivity analysis of the ISMEAR tag is shown in this section. The energy values obtained for different sigma values for the three smearing options studied in this work were similar, hence the choice of the ISMEAR and SIGMA values were based on the computational time taken for the calculations.

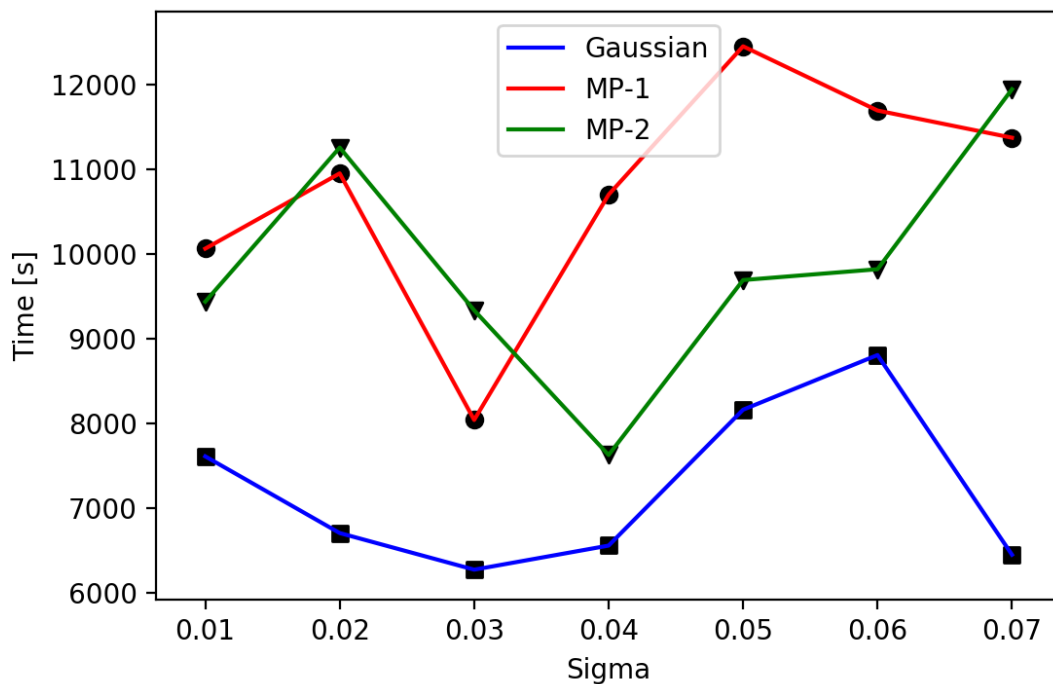


FIGURE D.1: Time taken for Gaussian, MP-1 and MP-2 smearing for a range of SIGMA values.

From Figure D.1 it is observed that Gaussian smearing takes lesser amount of computational time compared to the other options studied. A Gaussian smearing with a SIGMA value of 0.3 was chosen for the calculations in this work.

Appendix E

VASP Primer

This section provides information on how to start a DFT calculations in VASP. Follow the instructions in the article in the following link to install and start PuTTY: https://hpcwiki.tudelft.nl/index.php/How_to_log_in

Once the PuTTY applications is opened, a following screen will appear as in Figure E.1.

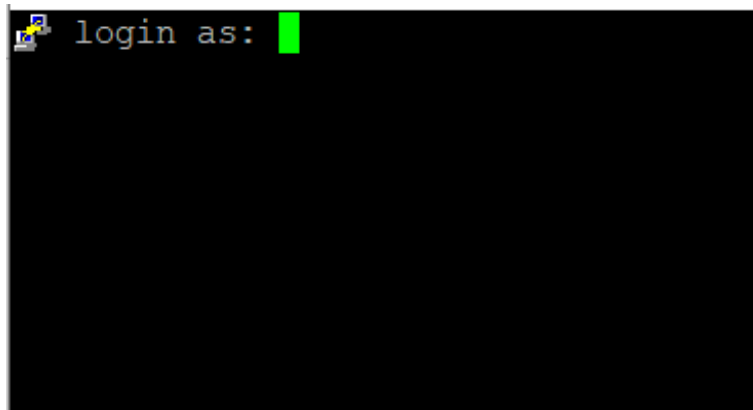


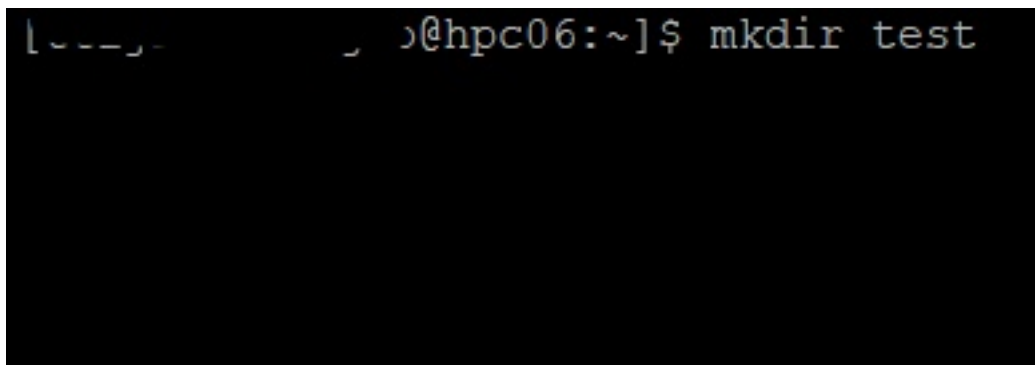
FIGURE E.1: Login window

After entering the username and password a following screen will appear with 'username@hpc06: ' written within the square brackets (I have blotted out my username in the Figure E.2)



FIGURE E.2: After login window

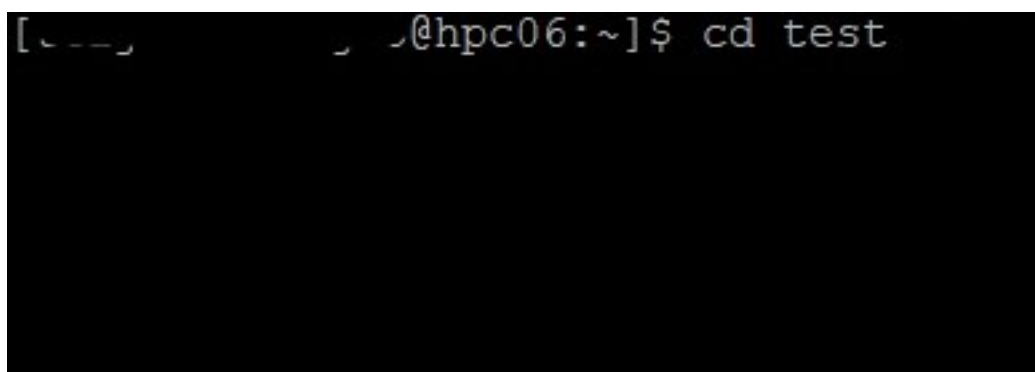
Create a directory with command `mkdir 'name of directory'` as shown in the Figure E.3. I have used a name 'test' for my directory.



```
[~]@hpc06:~]$ mkdir test
```

FIGURE E.3: Making a new directory

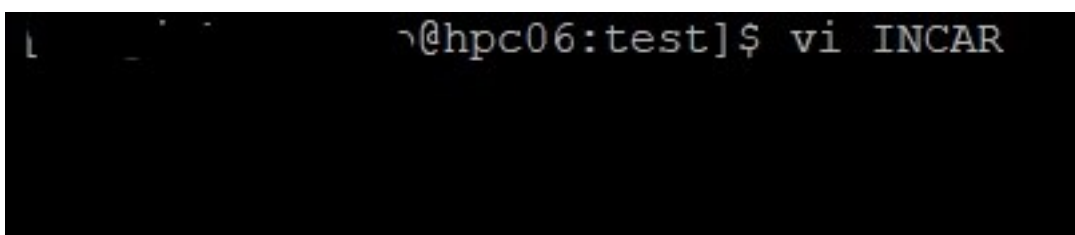
Once the directory is created, move into the directory by typing in `cd 'name of dir'` as shown in Figure E.4.



```
[~]@hpc06:~]$ cd test
```

FIGURE E.4: Changing directory

Once in the directory, create INCAR, KPOINTS, POSCAR files. You can create them by typing `vi 'name of the file'` as shown in Figure E.5.



```
[~]@hpc06:test]$ vi INCAR
```

FIGURE E.5: Creating files

To get an idea of how these files look, I have provided the INCAR, KPOINTS and POSCAR files that were used during this thesis work. Please make sure the tags chosen fits the study that is planned to be conducted. The POTCAR files will be provided by your supervisors. It must be noted that POSCAR for larger systems can be created by visualization softwares such as VESTA.

To start writing a file you have to type 'i' to get into insert mode. Once the files are created, you can exit by pressing the 'Esc' key and typing ':x'. This

```
striped_borophene
0
Monkhorst
5 5 1
0 0 0
```

FIGURE E.6: KPOINTS for pristine borophene

```
PREC = Accurate
ENCUT = 500
EDIFF = 10E-6
EDIFFG = -0.001
LREAL = Auto
IBRION = 2
ISYM = 0
IVDW = 1
NELMIN = 4
NSW = 500
ISIF = 4
ISMear = 0 ; SIGMA = 0.3
ENAUG = 650
```

FIGURE E.7: INCAR for pristine borophene

will take you back to your directory. Once all the four input files are present, you can create a submit job script which submits your job to the cluster. A sample submit job script is included below in Figure E.9. If there are visibility issues with Figure E.9, one can use Figure E.10.

After the submit job is created, come back to the directory with your input files and type in the command `qsub 'name of submitjob script'`. You can view the jobs running in the cluster with the command `qstat`.

```

New structure
1.0
      6.4672508240      0.0000000000      0.0000000000
      0.0003502441      14.3731603580      0.0000000000
      0.0788386970      -0.3057017383      30.2198418379

      B
      40
Direct
      0.999602139      0.000465040      0.999924898
      0.999687076      0.200648308      0.999657631
      0.999847054      0.400444597      0.999327540
      0.999868929      0.600501001      0.999230325
      0.999685764      0.800250173      0.999603570
      0.249672949      0.000462671      0.999914050
      0.249686331      0.200655043      0.999661744
      0.249659151      0.400439352      0.999417841
      0.249665067      0.600498676      0.999320090
      0.249671429      0.800228357      0.999605179
      0.499699265      0.000476705      0.999979913
      0.499678224      0.200643241      0.999668837
      0.499574780      0.400451809      0.999225616
      0.499569744      0.600488782      0.999131978
      0.499660790      0.800249696      0.999613106
      0.749625981      0.000478473      0.000014142
      0.749669015      0.200645551      0.999657691
      0.749762475      0.400461555      0.999135494
      0.749787986      0.600476027      0.999052644
      0.749659777      0.800229013      0.999596417
      0.124999717      0.099771790      0.970658541
      0.125072151      0.299650699      0.970080793
      0.125142351      0.499761969      0.969811738
      0.125073493      0.700003624      0.969959795
      0.124988660      0.899894714      0.970667362
      0.375039309      0.099777304      0.970631361
      0.374958426      0.299677372      0.970124066
      0.374906212      0.499775559      0.969924927
      0.374982893      0.699972808      0.970003664
      0.375024915      0.899886549      0.970643699
      0.625010073      0.099767402      0.970550358
      0.625009120      0.299651444      0.970213890
      0.624987423      0.499787271      0.970192671
      0.625018299      0.700000465      0.970092833
      0.625001490      0.899907172      0.970586240
      0.874973774      0.099770300      0.970605016
      0.875112891      0.299681753      0.970181108
      0.875214696      0.499786437      0.970080614
      0.875098050      0.699973881      0.970060229
      0.874969900      0.899895310      0.970624864

```

FIGURE E.8: POSCAR for pristine borophene

```
#PBS -l nodes=1:ppn=4
#PBS -q mse
module load vasp/5.3.5-vtst
cd $PBS_O_WORKDIR
echo $PBS_O_WORKDIR
mpirun vasp > vasp.out
```

FIGURE E.9: Submit job script

```
#PBS -l nodes=1:ppn=4
#PBS -q mse
module load vasp/5.3.5-vtst
cd $PBS_O_WORKDIR
echo $PBS_O_WORKDIR
mpirun vasp > vasp.out
```

FIGURE E.10: Submit job script with white background

Bibliography

1. *Space Applications of Hydrogen and Fuel Cells* | NASA <https://www.nasa.gov/content/space-applications-of-hydrogen-and-fuel-cells>.
2. Mulder, M., Perey, P. & Moraga, J. L. Outlook for a Dutch hydrogen market.
3. *Transforming Oil Wells Into Carbon Free Hydrogen Sources [Interview]* <https://blog.ballard.com/green-hydrogen-sources>.
4. Züttel, A. Materials for hydrogen storage. *Materials Today* **6**, 24–33 (2003).
5. Lahnaoui, A., Wulf, C., Heinrichs, H. & Dalmazzone, D. Optimizing hydrogen transportation system for mobility via compressed hydrogen trucks. *International Journal of Hydrogen Energy* **44**, 19302–19312 (July 2019).
6. *Hydrogen Storage* | Department of Energy <https://www.energy.gov/eere/fuelcells/hydrogen-storage>.
7. Durbin, D. J. & Malardier-Jugroot, C. Review of hydrogen storage techniques for on board vehicle applications. *International Journal of Hydrogen Energy* **38**, 14595–14617 (2013).
8. LI, J. Q. *et al.* A theoretical analysis of temperature rise of hydrogen in high-pressure storage cylinder during fast filling process. *Advances in Mechanical Engineering* **12**, 1–10 (2020).
9. *IU South Bend Chemistry and Biochemistry: PPT* <http://iusbchemistry.blogspot.com/p/ppt.html>.
10. Perez, E. V., Balkus, K. J., Ferraris, J. P. & Musselman, I. H. Mixed-matrix membranes containing MOF-5 for gas separations. *Journal of Membrane Science* **328**, 165–173 (2009).
11. Shet, S. P., Shanmuga Priya, S., Sudhakar, K. & Tahir, M. A review on current trends in potential use of metal-organic framework for hydrogen storage. *International Journal of Hydrogen Energy* **46**, 11782–11803 (Mar. 2021).
12. Wong, J., Yadav, S., Tam, J. & Singh, C. V. A van der Waals density functional theory comparison of metal decorated graphene systems for hydrogen adsorption. *The Journal of Chemical Physics* **115**, 224301–224311 (2014).
13. Yadav, S., Tam, J. & Singh, C. V. A first principles study of hydrogen storage on lithium decorated two dimensional carbon allotropes. *International Journal of Hydrogen Energy* **40**, 6128–6136 (2015).
14. Seydou, M. *et al.* A DFT-D study of hydrogen adsorption on functionalized graphene. *RSC Advances* **5**, 14400–14406 (2015).

15. Ambrusi, R. E., Luna, C. R., Juan, A. & Pronsato, M. E. DFT study of Rh-decorated pristine, B-doped and vacancy defected graphene for hydrogen adsorption. *RSC Advances* **6**, 83926–83941 (Sept. 2016).
16. Garara, M. *et al.* Phosphorene: A promising candidate for H₂ storage at room temperature. *International Journal of Hydrogen Energy* **44**, 24829–24838 (Sept. 2019).
17. Li, Q. F., Wan, X. G., Duan, C. G. & Kuo, J. L. Theoretical prediction of hydrogen storage on Li-decorated monolayer black phosphorus. *Journal of Physics D: Applied Physics* **47**, 465302–465308 (Nov. 2014).
18. Zhe Sheng, Shujing Wu, Xianying Dai, Tianlong Zhao & Yue Hao. A first-principles study of hydrogen storage capacity based on Li–Na-decorated silicene. *Physical Chemistry Chemical Physics* **20**, 13903–13908 (May 2018).
19. Wang, J., Li, J., Li, S.-S. & Liu, Y. Hydrogen storage by metalized silicene and silicane. *Journal of Applied Physics* **114**, 124309–124313 (Sept. 2013).
20. Süleyman, E., De Wijs, G. A. & Brocks, G. DFT study of planar boron sheets: A new template for hydrogen storage. *Journal of Physical Chemistry C* **113**, 18962–18967 (2009).
21. Peng, B. *et al.* Stability and strength of atomically thin borophene from first principles calculations. *arXiv* **5**, 399–407 (2017).
22. Wang, Z. Q., Lü, T. Y., Wang, H. Q., Feng, Y. P. & Zheng, J. C. Review of borophene and its potential applications. *arXiv* **14**, 33403–33422 (2019).
23. Haldar, S., Mukherjee, S. & Singh, C. V. Hydrogen storage in Li, Na and Ca decorated and defective borophene: A first principles study. *RSC Advances* **8**, 20748–20757 (2018).
24. Li, L., Zhang, H. & Cheng, X. The high hydrogen storage capacities of Li-decorated borophene. *Computational Materials Science* **137**, 119–124 (2017).
25. Wen, T. Z., Xie, A. Z., Li, J. L. & Yang, Y. H. Novel Ti-decorated borophene χ_3 as potential high-performance for hydrogen storage medium. *International Journal of Hydrogen Energy* **45**, 29059–29069 (2020).
26. Baraiya, B. A. *et al.* Nitrogen-decorated borophene: An empowering contestant for hydrogen storage. *Applied Surface Science* **527**, 146852–146860 (2020).
27. Chen, X., Wang, L., Zhang, W., Zhang, J. & Yuan, Y. Ca-decorated borophene as potential candidates for hydrogen storage: A first-principle study. *International Journal of Hydrogen Energy* **42**, 20036–20045 (2017).
28. Q, L. *et al.* Synthesis of borophane polymorphs through hydrogenation of borophene. *Science (New York, N.Y.)* **371**, 1143–1148 (Mar. 2021).
29. Qin, G., Du, A. & Sun, Q. A theoretical insight into a feasible strategy for the fabrication of borophane. *Physical Chemistry Chemical Physics* **20**, 16216–16221 (June 2018).
30. Karim, W. *et al.* Catalyst support effects on hydrogen spillover. *Nature* **2017** 541:7635 **541**, 68–71 (Jan. 2017).

31. Martinez, J.-P. The Hartree-Fock method: from self-consistency to correct symmetry. *Annalen der Physik* **529**, 1600328–1600333 (Jan. 2017).
32. Kryachko, E. S. & Ludeña, E. V. The Thomas-Fermi Energy Density Functional and Its Generalizations. *Energy Density Functional Theory of Many-Electron Systems* **4**, 312–410 (1990).
33. Dirac, P. A. M. Note on Exchange Phenomena in the Thomas Atom. *Mathematical Proceedings of the Cambridge Philosophical Society* **26**, 376–385 (1930).
34. LeSar, R. *Introduction to computational materials science: fundamentals to applications* English (Cambridge University Press, 2013).
35. Haunschild, R., Barth, A. & French, B. A comprehensive analysis of the history of DFT based on the bibliometric method RPYS. *Journal of Cheminformatics* 2019 11:1 **11**, 1–15 (Nov. 2019).
36. Hohenberg, P. & Kohn, W. Inhomogeneous Electron Gas. *Phys. Rev.* **136**, B864–B871 (Nov. 1964).
37. Kohn, W. & Sham, L. J. Self-Consistent Equations Including Exchange and Correlation Effects. *Phys. Rev.* **140**, A1133–A1138 (Nov. 1965).
38. Lee, J. G. T. A. T. T. *Computational materials science : an introduction* English. Boca Raton, 2017.
39. Perdew, J. P., Burke, K. & Ernzerhof, M. Generalized Gradient Approximation Made Simple. eng. *Physical review letters* **77**, 3865–3868 (Oct. 1996).
40. Sholl, D. S. & Steckel, J. A. *Density Functional Theory: A Practical Introduction* 1–238 (John Wiley and Sons, Aug. 2009).
41. Henkelman, G., Uberuaga, B. P. & Jónsson, H. A climbing image nudged elastic band method for finding saddle points and minimum energy paths. *The Journal of Chemical Physics* **113**, 9901–9904 (Nov. 2000).
42. VASP <https://cmp.univie.ac.at/research/vasp/>.
43. Grimme, S. Semiempirical GGA-type density functional constructed with a long-range dispersion correction. *Journal of Computational Chemistry* **27**, 1787–1799 (Nov. 2006).
44. *Transition State Tools for VASP — Transition State Tools for VASP* <https://theory.cm.utexas.edu/vtsttools/>.
45. Chen, X. *et al.* First-Principles Study on the Mechanism of Hydrogen Decomposition and Spillover on Borophene. *Journal of Physical Chemistry C* **121**, 17314–17320 (Aug. 2017).